Mechanisms by Which Gulf of Guinea and Eastern North Atlantic Sea Surface Temperature Anomalies Can Influence African Rainfall

EDWARD K. VIZY AND KERRY H. COOK

Department of Earth and Atmospheric Sciences, Cornell University, Ithaca, New York

(Manuscript received 1 October 1999, in final form 18 May 2000)

ABSTRACT

The sensitivity of precipitation over West Africa to sea surface temperature anomalies (SSTAs) in the Gulf of Guinea and the eastern North Atlantic is studied using a GCM. Results from nine perpetual July simulations with various imposed SSTAs are presented and analyzed to reveal associations between the precipitation and SST fields via large-scale circulation and atmospheric moisture anomalies.

Rainfall increases over the Guinean Coast and decreases over the Congo basin when warm SSTAs are present in the Gulf of Guinea. These precipitation perturbations are related to the forcing of a Kelvin and a Rossby wave. The former is associated with a weakening of the Walker circulation, while the latter strengthens the West African monsoon. Rainfall over West Africa is less sensitive to cold SSTAs than to warm anomalies. Three contributing factors are identified as follows: 1) latitude of the SST forcing, 2) background flow, and 3) nonlinearity of the Clausius–Clapeyron equation (no more than a 20% effect). Despite the relative insensitivity to eastern North Atlantic SSTAs alone, a superposition of the individual responses to SSTAs is shown to be a poor predictor of the response to combined SSTAs, especially over central northern Africa.

A comparison of the modeled moisture budget anomalies to the difference between the summer seasons of 1988 and 1994 from the satellite observations and the NCEP reanalysis is conducted. While there may be many causes of precipitation differences between two particular years, the moisture budget anomalies are similar in that enhanced precipitation along the Guinean coast is supported mainly by low-level wind convergence from the south. The role of advection is also similar in the model and the reanalysis. However, the precipitation decrease over the Congo Basin that is associated with the Kelvin wave response to Gulf of Guinea SSTs in the model is not evident in the observations for these 2 yr.

1. Introduction

Since the mid-1960s annual rainfall has been predominantly below normal across much of West Africa. In particular, the Sahel, a semiarid region of West Africa between 10° and 20°N, has been plagued by deficient rainfall and drought conditions (Nicholson 1993). The scientific community is currently working to understand if this dry period represents change or variability, and how the precipitation differences are related to sea surface temperatures (SSTs), land surface conditions, and features of the large-scale circulation.

In this paper we consider only the effect of SST anomalies (SSTAs). Dryness over Sahelian Africa has been associated statistically with SSTAs on a global scale. We are concerned with only a portion of the possible effects of SST on West African precipitation, namely, SSTAs in the eastern Atlantic Ocean. Using GCM simulations and an examination of the National Centers for Environmental Prediction (NCEP) reanalysis, we explore the mechanism(s) that physically connect SST anomalies in the eastern Atlantic, including the Gulf of Guinea, with the precipitation field through the large-scale atmospheric hydrodynamics.

Several empirical studies suggest that there is a statistically significant relation between sub-Saharan precipitation and global-scale SST distributions. Lamb (1978) found that during the deficient rainy season of 1968 over the Sahel, warm SSTAs were present in the equatorial Atlantic, and during the abundant rainy season of 1967 over the Sahel, cool SSTAs were present in the equatorial Atlantic. Lamb and Peppler (1992) found a distinctive SSTA pattern over the Atlantic when comparing three of the driest years since 1940 (1972, 1977, and 1984) to the climatology, but the pattern broke down for the 1983 drought year. Folland et al. (1986, 1991) also identified a relationship between Atlantic SSTs and Sahelian precipitation, but they found a stronger correlation between African precipitation and ''global'' SSTs. In attempts to classify types of drought patterns, Fontaine and Bigot (1993) and Fontaine and Janicot (1996) identified four different SSTA patterns that

Corresponding author address: Dr. Edward K. Vizy, Department of Earth and Atmospheric Sciences, Cornell University, 3152 Snee Hall, Ithaca, NY 14853.
E-mail: ekv3@cornell.edu

were associated with West African rainfall. The modeling studies of Rowell et al. (1992) and Palmer et al. (1992) suggest that ocean forcing dominates the rainfall variability over the sub-Sahara, in agreement with the empirical studies. Overall, there is agreement among these empirical studies that SST distributions are related to West African rainfall variability. However, the physical basis for these correlations and their ramifications are not yet fully understood.

Other empirical studies have focused on the influence of more localized SSTAs, for example, in the Gulf of Guinea and the eastern Atlantic. Newell and Kidson (1984) and Cadet and Nnoli (1987) discussed the importance of the Gulf of Guinea for providing a supply of precipitable water to interior regions of Africa in the summer. Bah (1987) found that reduced summer Sahelian rainfall occurs in conjunction with warm SSTAs in the Gulf of Guinea in his composite created from the dry years (1948, 1949, 1968, 1970, 1971, and 1972), but that the reverse relationship does not hold for the anomalously wet year composite (1946, 1950, 1952, 1953, 1954, 1955, 1957, 1958, and 1966). Ward (1998) suggested that Atlantic SSTs are important in predicting rainfall fluctuations over the Guinean coast. In a modeling study, Druyan and Koster (1989) suggest that the Atlantic Ocean, due west of Sahelian Africa, is a major source of water vapor for western Sahel in both wet and dry years, but the Gulf of Guinea is an important source of moisture for this region only during wetter than normal years. Other modeling studies have associated drier seasons with a weaker cross-equatorial monsoonal flow (Lamb and Peppler 1990; Semazzi et al. 1993). Wagner and Da Silva (1994) observed that during the summer of wet years near the Guinea coast, there was a less developed cold tongue in the Gulf of Guinea along with a relaxation of the trade winds. All of these studies agree that the Gulf of Guinea is important in influencing rainfall over the Sahel, but the role of the northern Atlantic Ocean basin is still unclear.

Several studies have examined relationships between SST forcing and low-level dynamics of the atmosphere. Using composites derived from the 1948 to 1978 observational data, Janicot (1992) found that many near-equatorial atmospheric features [i.e., locations of subtropical high pressure centers, zones of maximum convergence, and the intertropical convergence zone (ITCZ) precipitation] were displaced southward during dry years over West Africa. However, empirical studies by Shinoda (1990a,b) and Shinoda and Kawamura (1994) found during the period of 1900 through 1987 that a reduction in rainfall intensity was more responsible for the reduced Sahelian rainfall than an equatorward retraction of the ITCZ. Dynamical features that have been associated with dry (wet) conditions across the Sahel include a weaker (stronger) tropical easterly jet in the upper troposphere, and a stronger (weaker) African easterly jet at the top of the boundary layer (Newell and Kidson 1984; Fontaine and Janicot 1992). In a modeling study, Druyan (1991) associated warm SSTs over the equatorial and southern Atlantic with reduced surface pressures over the South Atlantic, which reduced water vapor flow into western Africa. Druyan and Hastenrath (1991, 1992) associated increased rainfall during the summer of 1950 with a stronger penetration of the southerly flow off the Gulf of Guinea onto West Africa, consequently enhancing the moisture convergence over the Sahel. Rowell et al. (1992) found that the reduction in Sahelian rainfall in the summers of 1984 and 1987 was linked to weaker low-level moisture convergence, but the reduction in rainfall in 1983 was related to abnormally strong midlevel moisture divergence. Furthermore, the wet years of 1950 and 1958 were associated with a reduction of midlevel divergence of moisture.

The influence of surface conditions has also been explored. Nicholson (1989) discussed the possible roles of land surface parameters for strengthening or prolonging drought episodes in Africa. She suggested that changes in vegetation cover, evapotranspiration, albedo, and/or soil moisture can lead to modifications in latent and sensible heat transfer, thermal stability, and convergence fields in the atmosphere, influencing rainfall patterns over West Africa. Cook (1994a,b) identified three mechanisms that may be responsible for communicating between the surface and the precipitation field in West Africa. In one mechanism, surface warming generates increased dry convection, which increases (moisture) convergence over the land and enhanced rainfall. Second, lower-atmospheric warming results in decreased relative humidity, decreased low-level condensation, and decreased (moisture) convergence and rainfall. Finally, enhanced midtropospheric condensation drives low-level moisture convergence. These mechanisms together regulate rainfall over the continent. According to these two studies, it is necessary to have an understanding of the sensitivity of the atmosphere to the underlying surface in order to fully explain the precipitation variability of West Africa.

The purpose of this research is to understand the response of the precipitation field and features of the large-scale circulation over West Africa in a climate model to SSTAs in the Gulf of Guinea and the eastern North Atlantic Ocean in boreal summer. We are not implying that Atlantic SSTAs solely explain anomalous rainfall and circulation modifications over West Africa. However, the response to regional SSTAs is an integral part of the complete picture of West African rainfall sensitivity to global SSTAs, and it is a part that can be understood clearly by considering the low-level dynamics.

An atmospheric GCM is used to perform a series of simulations designed to isolate the response to SSTAs off the West African coast by using simplified boundary conditions. Then, with an understanding of the mechanisms that are important in the idealized model, observations of certain dry and wet years in West Africa are examined for evidence of similar mechanisms at

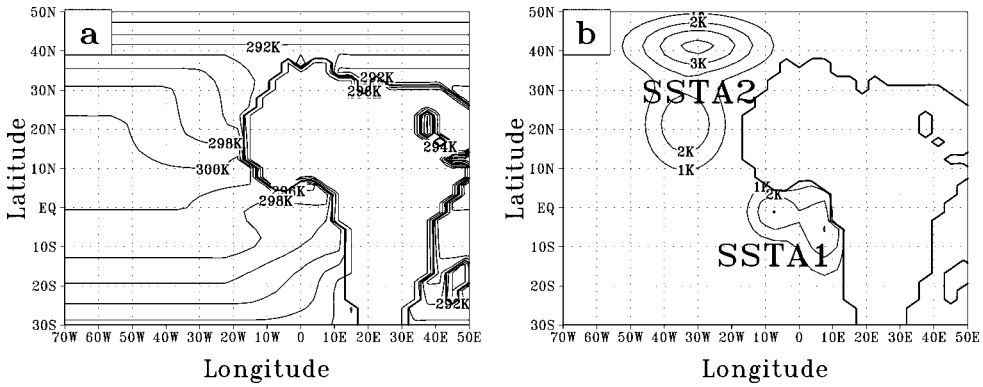

FIG. 1. (a) Control simulation SST distribution, and (b) SSTA patterns in the GCM simulations. Contours are in K.

work. Note the priority of this paper is to provide a thorough analysis of the physical mechanisms that may be important in the response of West African precipitation to regional SSTAs. The comparison of modeled results with observations is meant only as a validation of these results and not necessarily a complete explanation for the contrasting rainfall patterns between the wet and dry years chosen, since other factors are contributing.

A description of the GCM and how it is used is given in section 2, while section 3 discusses the diagnostic technique utilized in this investigation. Section 4 compares the boreal African precipitation in the GCM with observations. Sections 5 and 6 discuss the atmospheric response to Gulf of Guinea and eastern North Atlantic SSTAs, respectively, while section 7 explores the atmospheric response to the combined Gulf of Guinea–eastern North Atlantic SSTA cases. Section 8 compares the mechanisms identified in the GCM simulations to conditions observed during the summers of 1988 and 1994. The results are summarized in section 9.

2. Model and experiments

The model used for this study is a version of the GCM developed and maintained by the Climate Dynamics Group at the National Oceanic and Atmospheric Administration's Geophysical Fluid Dynamics Laboratory. It is a spectral model with R30 resolution corresponding to a grid resolution of 2.25° lat × 3.75° long, yielding 32 grid points over the West African Sahel. This model solves the primitive equations plus a prognostic equation for water vapor mixing ratio on 14 vertical levels in sigma coordinates. The model is fully nonlinear and contains feedbacks between the dynamics and physics. Cumulus convection is parameterized by means of a moist convective adjustment.

In order to isolate the effects of SSTAs on the West African climate, simplified surface boundary conditions have been adopted. The only landmass included at the surface is a flat version of Africa. The rest of the globe is set to ocean conditions. The surface drag coefficient used in the bulk aerodynamical parameterizations of sensible and latent heat fluxes from the surface are 0.001 over the ocean and over land 0.003. The model is run in a ''perpetual July'' mode to efficiently produce a climatology. Note, a climatology of similar duration generated from a seasonal mode simulation would require an integration period of over 100 yr. Soil moisture does not respond to the precipitation field, but is held fixed over Africa at climatological July conditions from Mintz and Walker (1993), and solar insolation represents mid-July conditions. Clouds are fixed at observed annual mean values, and their distribution is zonally uniform. Diurnal solar forcing is not included, and sea ice is not allowed to form. Ozone concentrations are also zonally uniform and hemispherically symmetric.

Nine simulations are discussed. Each is 3800 (model) days long, with the first 200 days devoted to spinup from an isothermal, dry atmosphere at rest. The last 3600 days are averaged to form the climatology. The model time step is 16 min, and variables are sampled daily. Different prescribed SSTs distinguish the nine GCM integrations. In the control integration, the observed climatological SST distribution from Shea et al. (1990) is prescribed off the west coast of Africa (45°N and 45°S) and zonally uniform July SSTs cover the rest of the ocean (Fig. 1a). Observed climatological SSTs are chosen for the Atlantic so the SST distribution can be as realistic as possible near West Africa, where SSTAs are to be superimposed. Zonally uniform SSTs are chosen for the rest of the ocean to represent summer conditions as closely as possible in the absence of other continents and their features.

In eight GCM simulations, perturbations are imposed on the background SST distribution (Fig. 1a) in the Gulf of Guinea and the eastern Atlantic. Observed SSTs from Shea et al. (1990) for the summers of 1988 and 1994 were used as a guide for determining the positions and magnitudes of the SSTAs. Preliminary simulations in which the idealized SSTAs had magnitudes similar to the observed resulted in weak response in the model.

TABLE 1. GCM simulation descriptions.

Integration name	Imposed SSTA
Control	None
Warm Gulf of Guinea	SSTA1
Cold Gulf of Guinea	−SSTA1
Warm eastern North Atlantic	SSTA2
Cold eastern North Atlantic	−SSTA2
Warm gulf–cold eastern N. Atlantic	SSTA1 and −SSTA2
Cold gulf–warm eastern N. Atlantic	−SSTA1 and SSTA2
Warm gulf–warm eastern N. Atlantic	SSTA1 and SSTA2
Cold gulf–cold eastern N. Atlantic	−SSTA1 and −SSTA2

In order to produce a diagnosable response with reasonable integration times, magnitudes of the SSTAs obtained from the NCEP reanalysis were increased approximately by a factor of 3. Figure 1b shows the SSTA patterns. Description of the location(s) and sign(s) of the Gaussian-shaped SSTAs for each simulation is shown in Table 1. All eight possible combinations of SSTAs in the Atlantic are simulated.

3. Atmospheric moisture budget

To relate structure of the precipitation field to features of the large-scale circulation, we examine the atmospheric water vapor budget. Using the approach employed by Lenters and Cook (1995), we partition the water vapor budget so that the climatological precipitation rate $\overline{P}$ (in mm day^{-1}), is equal to the evaporation rate, $\overline{E}$, minus the vertically integrated sum of the water vapor flux divergence and the local rate of change of water vapor mixing ratio according to

$$\overline{P} = \overline{E} - \overline{\int_0^1 p_s \left[\nabla_{3p} \cdot q\mathbf{u}_{3p} + \left(\frac{\partial q}{\partial t} \right)_p \right] \frac{d\sigma}{g\rho_w}}. \quad (1)$$

Here, p_s is the surface pressure, ∇_{3p} is the three-dimensional divergence operator in pressure coordinates, q is the water vapor mixing ratio, $\mathbf{u}_{3p}$ is the three-dimensional wind velocity, g is the acceleration due to gravity, ρ_w is the density of water, and $d\sigma$ is the sigma-level thickness. In the time mean, the third term on the rhs of Eq. (1) can be neglected as

$$\overline{p_s \frac{\partial q}{\partial t} \frac{d\sigma}{g\rho_w}} \sim 0. \quad (2)$$

Decomposing Eq. (1) into time mean and transient components, expanding the divergence operator into horizontal and vertical components, evaluating the vertical derivative, and rewriting the integral as a finite sum yields

$$P = C + A + O + T + E, \quad (3)$$

where all the variables in Eq. (3) represent climatological means, and

$$C = -\frac{p_s}{g\rho_w} \sum_{\sigma=0}^{1} (q\nabla_{2p} \cdot \mathbf{u}_2)\Delta\sigma, \quad (4)$$

$$A = -\frac{p_s}{g\rho_w} \sum_{\sigma=0}^{1} (\mathbf{u}_2 \cdot \nabla_{2p} q)\Delta\sigma, \quad (5)$$

$$O = -\frac{1}{g\rho_w}(q\omega)_s, \quad \text{and} \quad (6)$$

$$T \approx -\frac{1}{g\rho_w}\nabla_2 \cdot \left[\int_0^1 (\overline{p_s q \mathbf{u}_2} - \overline{p}_s \overline{q}\,\overline{\mathbf{u}}_2)\, d\sigma \right]. \quad (7)$$

[The overbar representing the time mean has been retained only in Eq. (7); see Lenters and Cook 1995 for more details.] Here C, or the ''moisture convergence term,'' represents precipitation associated with horizontal wind convergence in a moist environment, while A, the ''moisture advection term,'' represents precipitation associated with horizontal wind advection of moisture. The ''orographic term,'' O, is the vertical moisture flux into the bottom of an atmospheric p surface column, and it represents orographic precipitation. In these simulations $O = 0$.

4. Evaluation of African precipitation in the GCM

Before examining the influence SSTAs in the Atlantic have on rainfall rates over Africa in the model, the GCM's precipitation field and the moisture budget that determines the precipitation field are validated using the NCEP reanalysis (Kalnay et al. 1996), satellite observations, and station data.

Figure 2a shows the precipitation climatology from the GCM simulation with a featureless version of Africa alone. This simulation produces rainfall maxima of 10 mm day^{-1} over Cameroon (~10°N, 15°E), 18 mm day^{-1} over Ethiopia (~5°N, 40°E), and 6 mm day^{-1} over the Arabian peninsula (~20°N, 50°E). Over West Africa centered along 10°N rainfall rates are about 6 mm day^{-1}. Precipitation rates are low (less than 2 mm day^{-1}) over the equatorial Atlantic between 10° and 40°W.

Figure 2b shows the summer precipitation climatology from the satellite-gauge precipitation product of Huffman et al. (1995). The precipitation product is produced by using rain gauge reports to adjust a multisatellite estimate. The original data has a resolution of 2.5° × 2.5° but is interpolated to the GCM's resolution of 2.25° lat × 3.75° long. A climatology was created by averaging the summers of 1987 through 1997. There are three precipitation maxima over Africa, on the west coast, over Cameroon, and over Ethiopia. The far western maximum is centered just off the coast of West Africa (10°N, 15°W), with a magnitude of over 12 mm day^{-1}. The position of the Cameroon maximum in the satellite-derived product agrees with the GCM simulation. They both have magnitudes of about 10 mm day^{-1}. Unlike the GCM, the Ethiopia maxima is about 8 mm day^{-1} and precipitation rates over northeast Africa are

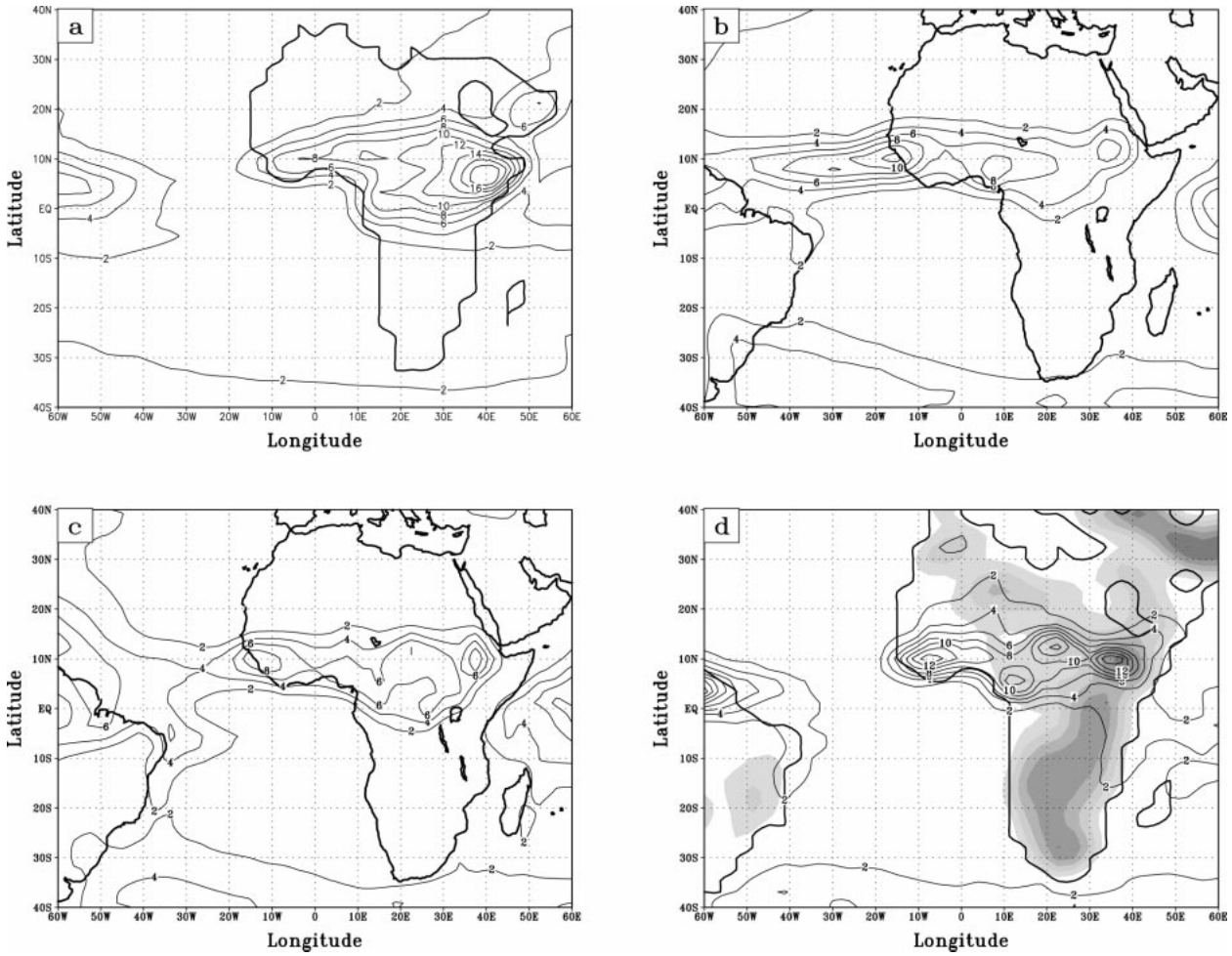

FIG. 2. Precipitation rates for (a) perpetual Jul control simulation, (b) satellite-gauge precipitation from Huffman et al. (1995), (c) NCEP 1949–98 summer climatology, and (d) R30 GCM with realistic surface features, including topography. Contour interval is 2 mm day^{-1}. Shading denotes the presence of topography above 400 m in height.

generally less than 2 mm day^{-1}. Rainfall rates of over 8 mm day^{-1} are found over the equatorial Atlantic, stretching from the West Coast of Africa to the northern tip of South America.

Figure 2c shows the 40-yr summer climatology from the NCEP reanalysis. The NCEP reanalysis climatology covers the years of 1949–98 and is also interpolated to the GCM's resolution. The rainfall maximum over far western West Africa is over 8 mm day^{-1} and centered at 10°N and 10°W. The Cameroon maximum is not present in the reanalysis. Instead, a broad band of over 6 mm day^{-1} rainfall rates stretches from 20°W to 30°E between the equator and 10°N. Rainfall rates over Ethiopia are over 8 mm day^{-1} and are displaced away from the east coast. Precipitation over the equatorial Atlantic has magnitudes weaker than the satellite-gauge magnitudes, but greater than the idealized GCM simulation.

A major difference between the GCM control simulation and the observations is that the control simulation produces less rainfall across far western West Africa and greater rainfall over East Africa than the observational climatologies (Figs. 2b and 2c). Also, higher rainfall rates in the GCM simulation extend too far north over Africa, especially over East Africa and the Arabian Peninsula. Precipitation is also very weak over the equatorial Atlantic.

Some of these differences are due to the simplified boundary conditions and some are associated with the well-known difficulties of simulating precipitation in global models. The addition of other continents in the GCM simulation decreases precipitation over East Africa and increases West African precipitation, improving the agreement with the other climatologies. Applying a realistic surface albedo and topography to the all-continent simulation (Fig. 2d) results in the West African rainfall maxima being focused over 10°N and 10°W, with a magnitude of over 14 mm day^{-1}. The GCM still produces very low rainfall over the equatorial Atlantic, and produces excessive rainfall over northern Africa. The Arabian precipitation maximum is a product of the

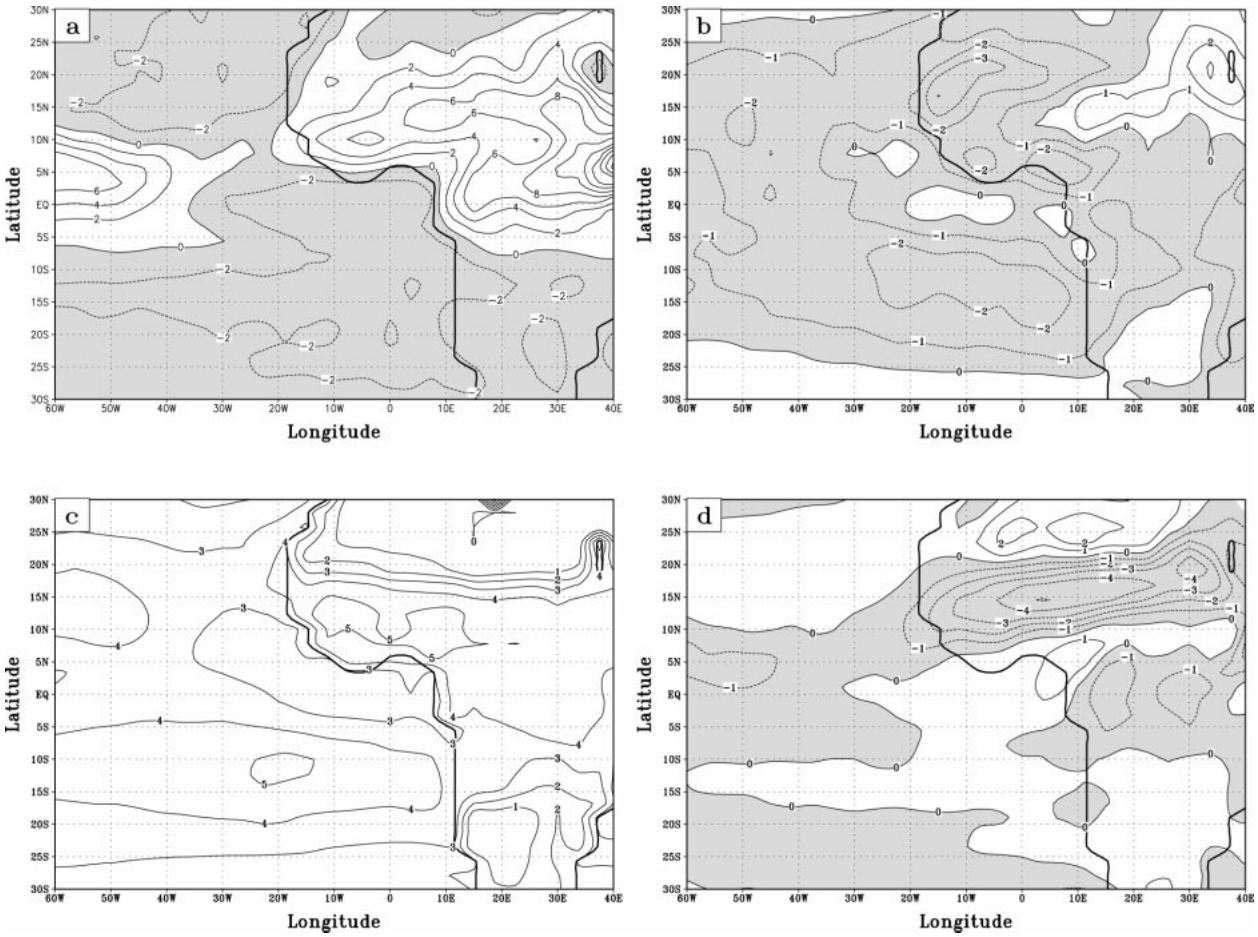

FIG. 3. (a) Convergence term [Eq. (4)], (b) advection term [Eq. (5)], (c) evaporation, and (d) transients term [Eq. (7)] from the control R30 GCM simulation. Units are mm day^{-1} and negative values are shaded.

simplified boundary conditions of the GCM, as is the positive zonal gradient in the precipitation across tropical Africa.

Overall, if more complex surface parameterizations are used, the simulated precipitation agrees better with the satellite-gauge and the NCEP reanalysis climatologies. The addition of topography and realistic surface albedo further improves the precipitation simulation. Discrepancies not associated with the simplified boundary conditions include the low rainfall over the equatorial Atlantic between 10° and 40°W, and the overproduction of precipitation over Saharan Africa.

Figure 3 shows the terms of the column moisture budget [Eq. (3)] for the GCM control simulation. Moisture convergence in the GCM (Fig. 3a) contributes positively toward precipitation over much of northern Africa and the tropical North Atlantic. The Ethiopian and Arabian rainfall maximas are accompanied by moisture convergence maximas larger than the rainfall maximas (by 3 mm day^{-1} and 6 mm day^{-1}, respectively). Over Cameroon and West Africa moisture convergence is about 2 mm day^{-1} smaller than the rainfall.

Moisture advection from Eq. (5) for the control simulation is shown in Fig. 3b. Negative moisture advection is present along the Guinean coast. A large moisture gradient exists between the Gulf of Guinea and West Africa as high mixing ratios are found along 12°N and lower mixing ratios are positioned over the gulf. The low-level southerly flow transports relatively drier air from the gulf over West Africa. Negative moisture advection is also found over northern and western Sahel between 20°W and 10°E. The northerly component of the low-level airflow transports dry Saharan air southward over the Sahel. Over the Sahel east of 10°E, positive moisture advection (1–2 mm day^{-1}) is present as the zonal flow transports the relatively wetter air over West Africa eastward.

Figure 3c is the evaporation field for the control simulation. The largest evaporation rates occur over tropical Africa, where rates exceed 5 mm day^{-1} over the Guinean coast. There is a sharp meridional gradient of evaporation over the Sahel, as rates are reduced from 4 mm day^{-1} over the southern Sahel (10°N) to less than 1 mm day^{-1} over the Sahara.

The transient eddies reduce the ITCZ's precipitation over northern Africa. Transient moisture flux vectors are directed away from each other along the axis of the mixing ratio maxima (along 12°N), resulting in the divergence over the Sahel and southern Sahara shown in Fig. 3d. Relatively humid air from the ITCZ is transported poleward toward the Sahara by the transient eddies. Negative moisture transients (about 1 mm day^{-1}) are also found over equatorial Africa, stretching into East Africa.

The boreal summer [June–August (JJA)] climatology from the NCEP reanalysis interpolated to the GCM's transform grid is compared with the GCM's moisture budget. Figure 4a shows the moisture convergence term [Eq. (4)] from the reanalysis. As in the idealized GCM (Fig. 3a), moisture convergence is positive over the Sahel. Even though the NCEP precipitation is smaller than the GCM precipitation in this region, the convergence term is about the same as in the reanalysis. A region of moisture divergence occurs over the Cameroon highlands in Central Africa, which is not present in the control simulation, but may be related to the tongue of reduced moisture convergence over the Cameroon Highlands produced in the GCM control (Fig. 3a). Unlike the GCM simulation, moisture convergence occurs over the Atlantic, west of Africa, increasing the rainfall over the eastern Atlantic.

The lack of moisture convergence over the eastern Atlantic in the GCM is associated with a stronger low-level westerly wind component over West Africa. The GCM's zonal moisture divergence is stronger over West Africa than in the reanalysis, lowering the overall moisture convergence.

As in the GCM, negative moisture advection (Fig. 4b) occurs along the Guinean coast and over the northern Sahel. Positive moisture advection of about 1 mm day^{-1} is present over the southern Sahel in the reanalysis, which is larger than the control simulation. The GCM only hints at this type of structure over the southern Sahel, west of 10°E. In both the reanalysis and the GCM, negative moisture advection (less than 3 mm day^{-1}) occurs over the eastern North Atlantic and the Gulf of Guinea.

The evaporation field for the reanalysis (Fig. 4c) compares favorably with the GCM simulation since the soil moisture is prescribed. The band of maximum evaporation is found over tropical Africa, north of the equator, with evaporation rates over the Guinean Coast weaker (1 mm day^{-1}) than the GCM. One important difference is the position of the meridional gradient of evaporation, which is about 5° lat farther north in the GCM.

The moisture transient term from the reanalysis is shown in Fig. 4d. Negative moisture transients over the Sahel in the reanalysis are about 2 mm day^{-1} weaker than in the GCM, and these extend southward over the Gulf of Guinea. As in the control simulation, positive transients are found over the Sahara in the reanalysis, but with smaller magnitudes.

Figure 4e shows the residual of the moisture budget balance for the reanalysis. This includes the orographic term, which is difficult to estimate for the reanalysis. The residual is positive along the Guinean Coast, indicating the possible importance of topographic effects of the highlands along the west coast of Africa in determining rainfall.

Discrepancies in moisture convergence and advection between the NCEP reanalysis and the GCM are due primarily to differences in the moisture field. Because moisture is not an assimilated variable, we use ground-based observations to validate. Figure 5a shows the summertime mixing ratio profile over Douala, Cameroon (4°N). The open-circled dashed line represents the National Center for Atmospheric Research RAOBS summer mixing ratio climatology (1956–64), while the closed-circle long dashed line represents the NCEP reanalysis mixing ratio for the same climatology period. The reanalysis reproduces the moisture profile over Douala accurately, in contrast to the GCM control simulation (solid line), which is drier throughout the atmosphere. For Niamey, Niger, at 13°N (Fig. 5b) the NCEP reanalysis mixing ratios are much larger in the lower and middle troposphere than both the RAOB and the GCM control simulation. The GCM still has a dry bias when compared to the observations; however, the moisture profile was more accurate than it was at Douala. For Tamanrasset, Algeria, at 22°N (Fig. 5c) the NCEP reanalysis has a wet bias in the lower and middle troposphere when compared to the observations and the GCM control. The GCM also has a wet bias at low levels. Overall, the NCEP reanalysis is too wet over Africa, especially over the Sahel and Sahara, and a cautious approach should be taken when comparing modeled results to the reanalysis. It is also apparent that the GCM has a dry bias, compared to the observations and the NCEP reanalysis.

Overall, the GCM reproduces structure that is comparable to the structure in the African observed precipitation field and in the atmospheric water vapor budget components in the reanalysis even with the model's simplified land-surface boundary conditions. This suggests that the GCM, with simplified boundary conditions to allow clearer analysis of the response to SSTAs, can be a valuable tool for identifying mechanisms by which the SSTAs in the eastern Atlantic Ocean influence rainfall across Africa.

5. Response to Gulf of Guinea SSTAs

Figure 6a shows the difference in rainfall between the warm Gulf of Guinea SSTA case and the control (Table 1). Rainfall is enhanced by up to 30% over West Africa between the Guinean Coast and 12°N. Rainfall is reduced by 1–2 mm day^{-1} along the equator between 10° and 40°E, and over Sahelian East Africa. Positive rainfall anomalies stretch westward along the equator

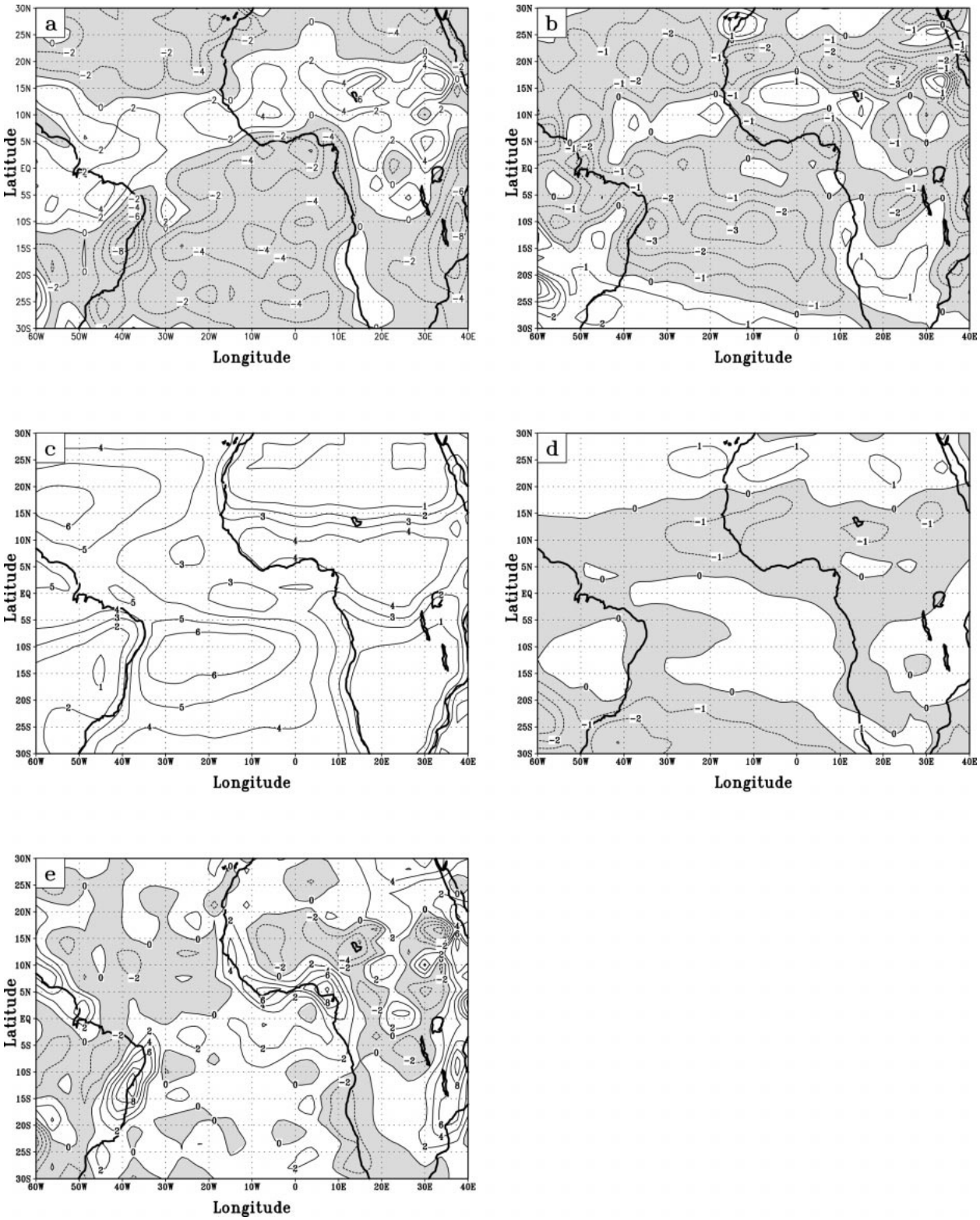

FIG. 4. (a) Moisture convergence term, (b) the moisture advection term, (c) the evaporation term, (d) the moisture transients term, and (e) the orographic term from the NCEP reanalysis 1949–98 summer (JJA) climatology. Units are mm day^{-1} and negative values are shaded.

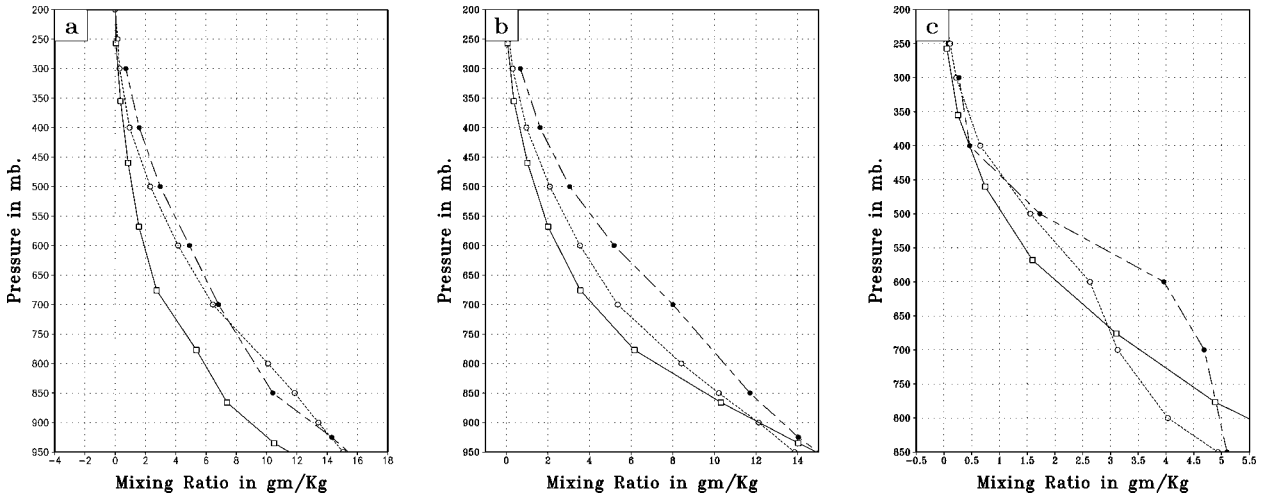

FIG. 5. Vertical profiles of mixing ratio for (a) Douala, Cameroon (at 4°N and 9°E); (b) Niamey, Niger (at 13°N and 2°E); and (c) Tamanrasset, Algeria (at 22°N and 5°E). The solid line in each panel represents the GCM control simulation mixing ratio and the open-circled dashed line represents the NCAR RAOB summer (JJA) mixing ratio climatology. The closed-circle long dashed line represents the NCEP reanalysis summer climatology. Units are g kg^{-1}.

to 70°W. Note that the rainfall anomalies do not reflect the structure or position of the SSTAs that caused them.

Cold SSTAs in the Gulf of Guinea produce precipitation anomalies of similar structure, but opposite sign and smaller magnitude. As shown in Fig. 6b, West African rainfall is reduced by only 10%–15% between the equator and 12°N, and the response at these latitudes over central Africa is very small. The sign and magnitude of the response over East Africa is the same as in the warm SSTA case. Precipitation rates are also reduced over the Atlantic along the equator. The only location with precipitation increases is equatorial central Africa, where precipitation rates are by up to 15% larger.

Figure 7 depicts anomalies from the control in the components of the atmospheric moisture budget for the simulations with warm (left column) and cold (right column) SSTAs in the Gulf of Guinea. Differences in the moisture convergence term, C [Eq. (4)], are shown in Figs. 7a and 7b; differences in the moisture advection term, A [Eq. (5)], are in Figs. 7c and 7d; differences in E are in Figs. 7e and 7f; and differences in T [Eq. (7)] are shown in Figs. 7g and 7h. The orographic term [Eq. (6)] anomalies are negligible, since the model has no topography, and are not shown.

In both the warm and cold SSTA simulations, anomalies in C (Figs. 7a and 7b) most closely resemble the rainfall anomalies (Figs. 6a and 6b) in spatial structure, but their magnitudes are about 1 mm day^{-1} larger than the precipitation anomalies. Differences in A and E do not account for this difference. These two terms have their largest differences directly over the SST anomalies in the gulf. Enhanced evaporation over the warm SSTAs (Fig. 7e) is balanced by column moisture divergence associated with advection (Fig. 7c) as the added at-

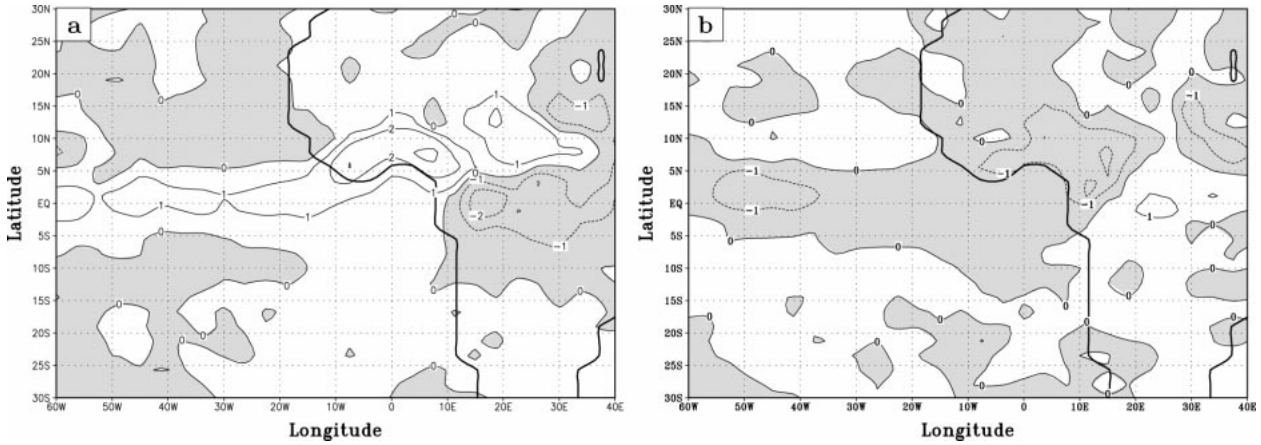

FIG. 6. Anomalous precipitation for (a) the warm Gulf of Guinea SSTA simulation minus the control and (b) the cold Gulf of Guinea SSTA simulation minus the control. Contour interval is 1 mm day^{-1}. Shading denotes negative perturbations.

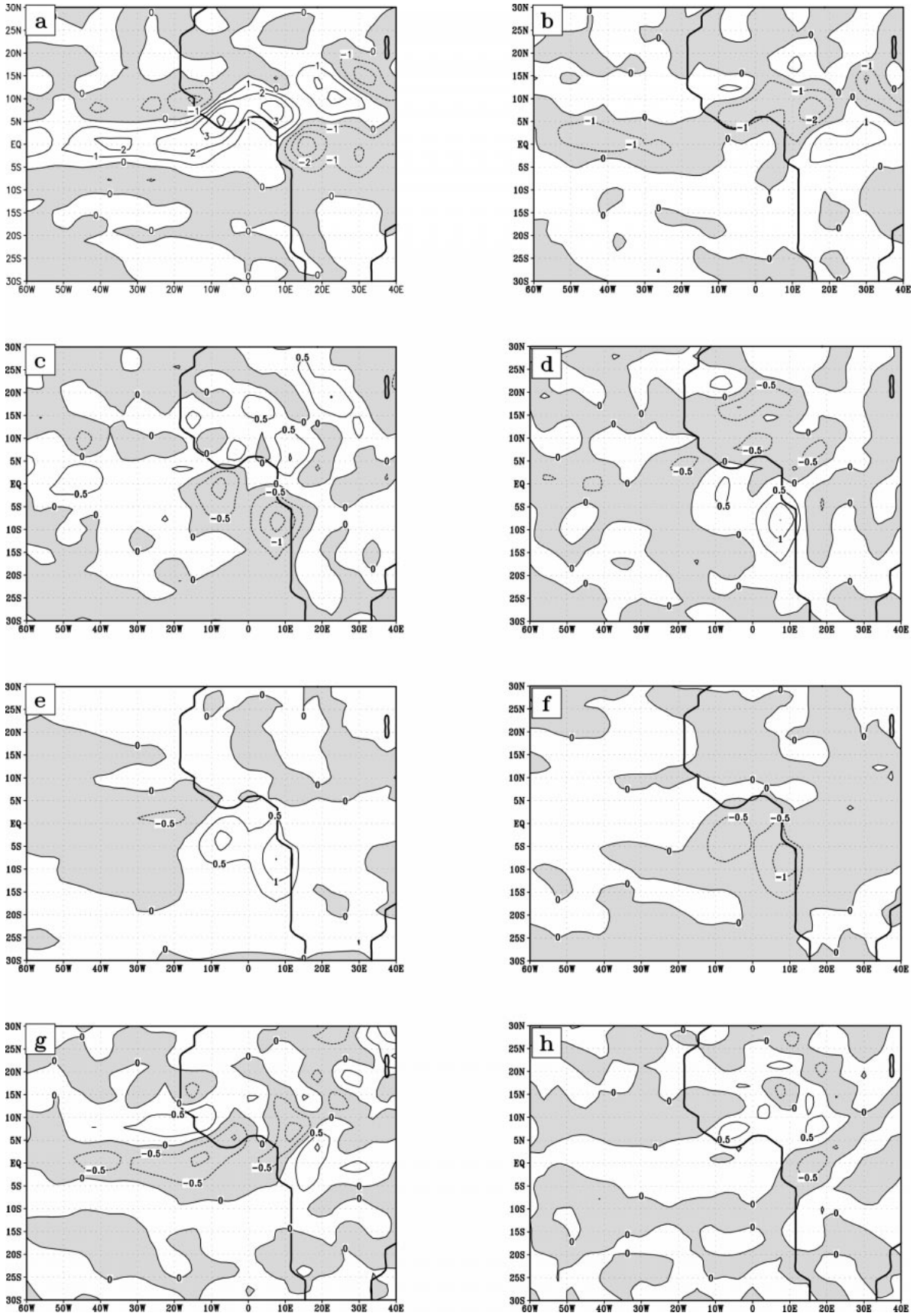
a
b
c
d
e
f
g
h
30N 25N 20N 15N 10N 5N EQ 5S 10S 15S 20S 25S 30S
60W 50W 40W 30W 20W 10W 0 10E 20E 30E 40E

mospheric moisture is transported northward instead of condensing over the gulf and increasing precipitation rates in the vicinity of the SSTAs. The opposite occurs in the cold SSTA case (Figs. 7d and 7f). Over West Africa, anomalies in A are generally under 1 mm day^{-1} and of the same sign as the convergence term anomalies, so they do not explain the discrepancy between the convergence term anomalies and the precipitation anomalies.

Differences in column moisture convergence by transient eddies oppose the differences in the convergence term anomalies, and account for the fact that the precipitation anomalies are smaller than the convergence term anomalies. This is especially clear over West Africa and the Atlantic in the warm SSTA case (Fig. 7g), in which reductions in moisture convergence by transient activity accompany increases in the convergence term (Fig. 7a). To the north, greater moisture convergence by transients balances reductions in the convergence term, so there is no response in the precipitation field on the coast near 10°N. In the cold SSTA case, anomalous moisture convergence due to transient activity is smaller, but the tendency to oppose the contributions from the moisture convergence and advection terms is the same.

Changes in the column moisture budget due to Gulf of Guinea SSTAs are related to differences in the moisture content of the atmosphere as well as the dynamical response of the atmosphere. The presence of the SSTAs is communicated from the sea surface into the atmosphere through the sensible heat flux and by evaporation (latent heating). Sensible heating modifies air temperatures in the lower troposphere near the SSTAs. Differences in evaporation change the low-level moisture content, but directly modify atmospheric temperature primarily in the middle and upper troposphere where condensation occurs. The heat absorbed in evaporating water can be deposited into the atmosphere over the SSTAs, or in some location far removed.

The amount of water vapor present in the atmosphere over the Gulf of Guinea and the Guinean coast is increased (reduced) in the warm (cold) SSTA case. Figure 8 shows mass-weighted, vertically integrated mixing ratio for the warm (Fig. 8a) and cold (Fig. 8b) SSTA cases. The amount of moisture increases over the warm Gulf of Guinea SSTAs, extending out over the Atlantic along the equator and penetrating onto the Guinean coast south of the ITCZ. Over the African Congo, the amount of water vapor in the atmosphere decreases.

The opposite occurs over the Gulf of Guinea and the Congo in the cold SSTA case, but with smaller magnitudes. Reduced moisture amounts are found over the northwestern Sahel in the cold SSTA case, but the opposite does not occur in the warm SSTA case. This reduction in water vapor in the cold SSTA case is associated with a stronger, more active African easterly jet, which removes water vapor from the atmospheric column below the level of condensation. In addition, possibly because of the nonlinearity of the Clausius–Clapeyron equation, the change in saturation vapor pressure and, therefore, evaporation, associated with a temperature decrease is smaller than that associated with a temperature increase. For example, the saturation vapor pressure increases by about 6 mb due to a temperature increase from 297 to 300 K, but decreases by only 5 mb for a temperature decrease from 297 to 294 K. Therefore, the magnitude of the vapor pressure anomaly is about 20% larger in the warm case. In addition, column moisture convergence by transient eddies is more important when SSTAs are cold, opposing anomalous moisture convergence to reduce the magnitude of the anomalous precipitation response. The differences in the magnitudes of the precipitation anomalies between the warm SSTA and cold SSTA cases are approximately 20%.

Figure 9a shows anomalous eddy geopotential and eddy winds at 866 mb due to warm SSTAs in the gulf. The well-known response to steady forcing near the equator from the shallow water equations is evident [e.g., see Fig. 11.19 in Gill (1982)]. The purely zonal flow into the heating anomaly close to the equator is the Kelvin wave response, and this is the only response to the east of the heating. It is associated with zonal divergence directly east of the SSTA (Fig. 7a) and precipitation reductions over equatorial Africa (Fig. 6a).

Kelvin and Rossby wave responses both occur to the west of the SSTA. The presence of the Rossby mode is indicated by the cyclonic anomaly near 12°N and 10°W, and meridional wind perturbations that occur in addition to the zonal wind perturbations of the Kelvin mode. The northward meridional wind perturbations between the Guinean coast and 20°N along the Greenwich meridian form part of the anomalous flow about the cyclone, and they strengthen the West African monsoon flow in this region. As in the shallow water solution to steady heating, the maximum vertical velocity perturbations are near the maximum meridional wind perturbations, in the southeast quadrant of the cyclonic perturbation. This places the vertical velocity perturbation associated with

←

FIG. 7. Anomalous moisture convergence term for (a) the warm Gulf of Guinea SSTA case and (b) the cold Gulf of Guinea SSTA case, anomalous moisture advection term for (c) the warm Gulf of Guinea SSTA case and (d) the cold Gulf of Guinea SSTA case, anomalous evaporation for (e) the warm Gulf of Guinea SSTA case and (f) the cold Gulf of Guinea SSTA case, and anomalous moisture transients for (g) the warm Gulf of Guinea SSTA case and (h) the cold Gulf of Guinea SSTA case. Contour interval is 0.5 mm day^{-1}, except for the moisture convergence term, where it is 1 mm day^{-1}. Shading denotes negative perturbations.

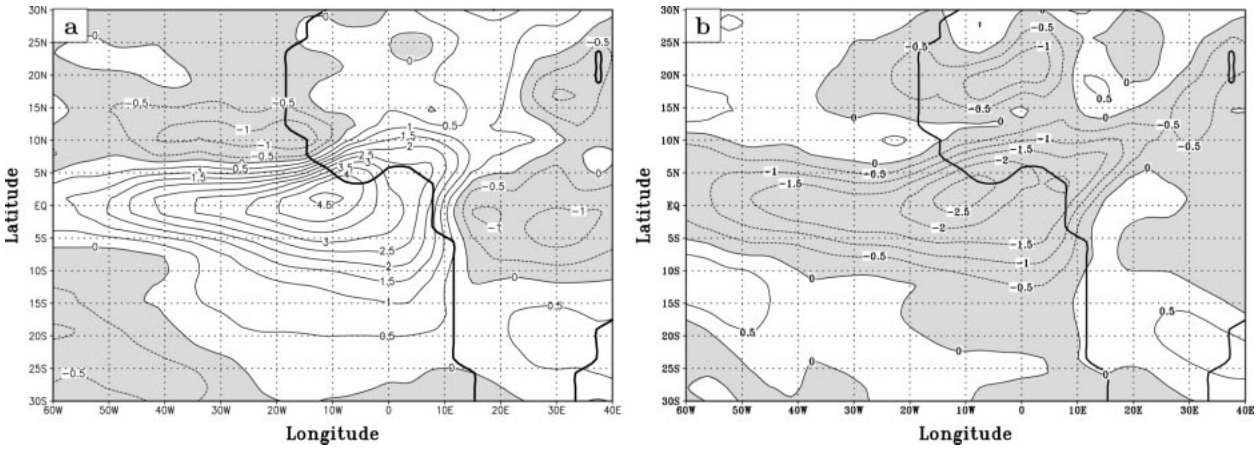

FIG. 8. Anomalous mass-weighted vertically integrated mixing ratio for the (a) warm Gulf of Guinea SSTA simulation minus the control, and (b) the cold Gulf of Guinea SSTA simulation minus the control. Contour interval is 0.5 kg_{H2O} m^{-2} with negative values shaded.

the Rossby mode along the Guinean coast, and enhanced precipitation in this region results.

The return flow of the Rossby wave response is the equatorward flow seen to the west of the heating anomaly. This return flow occurs over a wider region (from about 20° to 80°W) than the more concentrated poleward flow. The resulting convergence along the equator (Fig. 7a), in the more moist environment near the warm SSTA, leads to the precipitation enhancements across the equatorial Atlantic west of Africa (Fig. 6a).

The Kelvin wave response to Gulf of Guinea SSTAs is associated with the generation of an anticyclonic perturbation over northern Sudan (Fig. 9a). Zonal divergence directly east of the SSTA over equatorial Africa diverts the low-level moist inflow from the Indian Ocean that feeds the East African precipitation maximum. This results in a westward shift of the precipitation maximum, with reduced rainfall over western Sudan and Chad. It is likely that this response would be less prominent in a model with topography, since the Ethiopian highlands generate a strong orographic term in the column moisture budget.

Unlike the Gill model formulation, the response in the GCM is nonlinear and occurs in the presence of a complicated basic-state flow, most notably the West African monsoon and a Walker circulation on the equator. The westerly flow anomalies to the east of the SSTAs represent a weakening of the basic-state onshore flow in this region, and a weakening of the Walker circulation. This contributes to a reduction in the subsidence over the Gulf of Guinea, consistent with a decrease in the land–sea temperature contrast that accompanies a warming in the gulf. This subsidence is an important factor in determining the intensity of the West African monsoon. Because of this subsidence, rainfall is not enhanced over the SSTAs (Fig. 6a) but over the African coast to the north as explained by the column moisture budget (Fig. 7). Changes in evaporation are associated with modifications in low-level moisture levels. Subsidence over the gulf limits the vertical transport of the water vapor out of the boundary layer, and the moisture anomaly is advected northward by the low-level flow (Figs. 7c and 7d). The moisture anomaly is advected to the north, into West Africa because of purely dynamical constraints. The dynamical response to the midtropospheric condensational heating is the same as the one described by Cook (1997), namely, increased midtropospheric heating due to the moisture anomaly generates positive low-level vorticity tendencies between the Guinean coast and 10°N. The lower atmosphere adjusts by increasing the advection of lower absolute vorticity air from the Gulf of Guinea, while decreasing the advection of higher vorticity air from the Sahara, generating anomalous poleward flow over West Africa (Fig. 9a). In this way, the West African monsoon is strengthened despite the decrease in the land–sea temperature contrast that occurs when the gulf is warm.

The mechanism described above is responsible for the precipitation dipole between the Sahel and Guinean Coast found in observations (Janowaik 1988; Janicot 1992; Rowell et al. 1995). In association with the advection of absolute vorticity, low-level wind convergence increases over the Guinean coast and decreases over the Sahel, supporting the anomalous precipitation dipole. The negative precipitation anomaly signal over the Sahel is weak because the dry air advection into the ITCZ from the Sahara is also weak. This dynamical response is associated with the precipitation dipole between the Sahel and Guinean coast found in the observations.

One can imagine that a large enough positive SSTA in the gulf could weaken the Walker circulation and the subsidence enough so that convection would break through directly over the SSTA. In this case, the precipitation and SSTA anomalies would be coincident, and we could expect a decrease of precipitation along the Guinean coast instead of the increase seen with a more moderate SSTA.

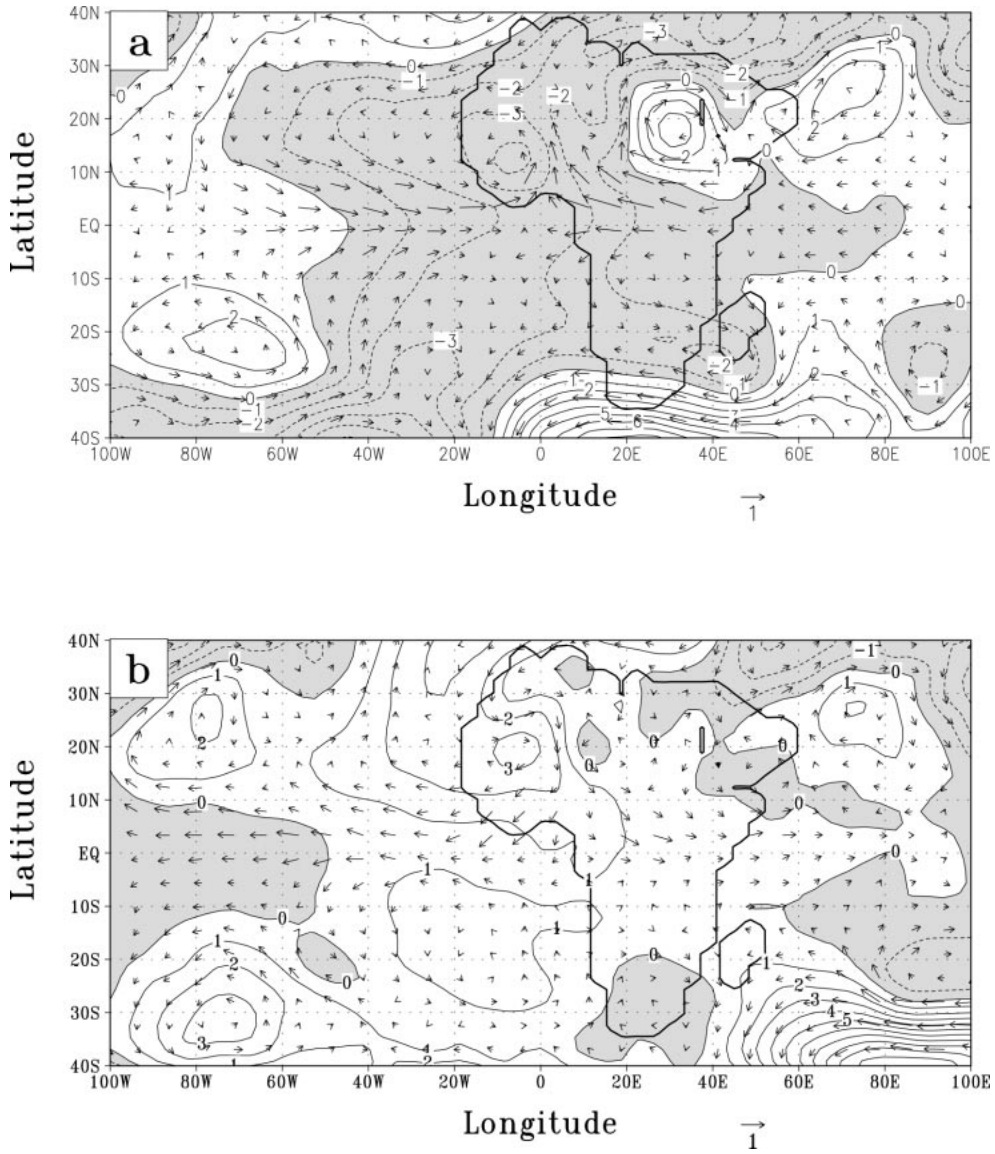

FIG. 9. (a) Warm Gulf of Guinea SSTA simulation minus the control, and (b) the cold Gulf of Guinea SSTA simulation minus the control 866-mb eddy geopotential and eddy wind. Units are gpm for eddy geopotential, m s^{-1} for the eddy wind. Negative eddy geopotential perturbations are shaded.

The opposite of the Gill response is seen in the atmosphere's response to cold SSTAs, and it explains the increase in precipitation over the Congo basin and the decrease over West Africa. The response is somewhat weaker since the moisture anomalies are not as large (Fig. 9b). Absent from the cold SSTA case is the anomalous anticyclonic response over northeastern Africa, even though rainfall is still reduced over the region. Westerly zonal wind perturbations of the low-level flow over equatorial Africa divert some of the moist low-level inflow from the Indian Ocean eastward, while weakening the onshore flow. The moisture content of the atmosphere (Fig. 8b) and condensational heating rates are reduced over Sudan and southern Egypt, but not to the extent they were in the warm Gulf of Guinea case because of the weaker atmospheric response to the cold SSTAs.

6. Response to eastern North Atlantic SSTAs

Figure 10a shows precipitation difference between the warm eastern North Atlantic SSTA case and the control simulation (Table 1). Rainfall is enhanced along 10°N from the Greenwich meridian to 60°W and over Sudan by about 1 mm day^{-1}. Over the Atlantic between the equator and 10°N from 60° to 80°W precipitation is reduced by about 1 mm day^{-1}. Rainfall is also reduced

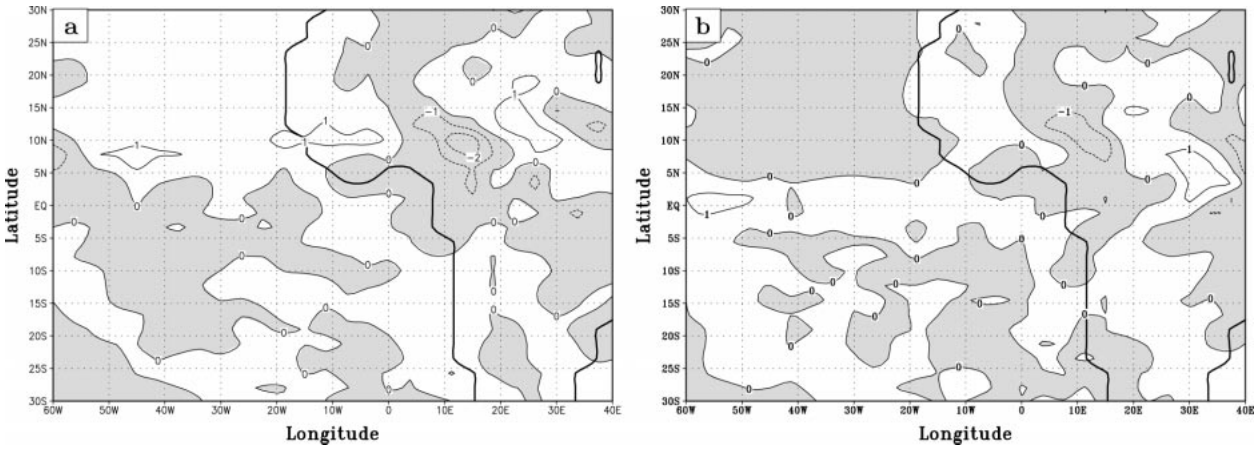

FIG. 10. (a) Warm eastern North Atlantic SSTA simulation minus the control, and (b) cold eastern North Atlantic SSTA simulation minus the control precipitation differences. Contour interval is 1 mm day^{-1}. Shading denotes negative perturbations.

by about 2 mm day^{-1} over Africa along 10°N between the Greenwich meridian and 20°E.

The cold SSTA case (Fig. 10b) is not exactly the opposite of the warm SSTA case over the Atlantic Ocean. Rainfall is reduced by about 0.5 mm day^{-1} along 10°N between the west coast of Africa and 70°W, and enhanced by about 1 mm day^{-1} along the equator. Over the African continent precipitation perturbations are also small and do not resemble the structure in Fig. 10a.

The precipitation perturbation magnitudes over the African continent in both SSTA cases are much smaller than the response to Gulf of Guinea SSTAs (Fig. 6), and symmetry between the warm and cold case responses is not present. When precipitation climatologies are formed from each half of the integration, the structure of the anomalous precipitation over much of the African continent is different between the first and the second halves. This suggests that even 3600-day means are not sufficient to capture any response, which must therefore be quite small. Over the North Atlantic, however, the two climatologies have the same structure and our analysis focuses on that region.

To understand why the atmospheric response to eastern North Atlantic SSTAs is weaker than the response to Gulf of Guinea SSTAs, consider the low-level circulation. Figure 11a shows the low-level flow at 866 mb from the control climatology. In association with the North Atlantic high, the summertime flow is northeasterly over northwest Africa. Westerly flow is present only north of 35°N. Since the thermal low over central Africa is centered at a lower latitude than the subtropical Atlantic high (20° vs 30°N), the continental circulation system also places easterly flow over much of northern Africa, especially in the west where westerlies do not occur north of 10°N. Thus, in contrast to the Gulf of Guinea case, the low-level flow is largely directed from Africa toward the eastern Atlantic, and this diminishes the influence of eastern Atlantic SSTAs.

Figure 11b shows the difference in eddy geopotential heights and winds at 866 mb between the warm eastern North Atlantic SSTA case and the control. The North Atlantic anticyclone is weaker when warm SSTAs are present in the eastern North Atlantic. Eddy geopotential heights are 5 gpm smaller in the center, and anomalous eddy flow indicates a reduction in circulation around the anticyclone. The anticyclone contracts and shifts to the west by about 5° of longitude. The strongest eddy height perturbations are in the midlatitudes of the Northern Hemisphere, north of the African continent. A low-level negative eddy geopotential perturbation is forced east of the heating center at 43°N. This response to low-level heating at midlatitudes agrees with the response predicted by linear theory (Hoskins and Karoly 1981). A negative eddy geopotential perturbation is also found over central northern Africa and is most likely an extension of the negative geopotential perturbation north of the African continent.

An examination of the thermodynamic budget shows that the atmosphere responds to the anomalous heating from the warm SSTAs near 40°N and 30°W by increasing cold air advection from the northwest into the heating region and increasing horizontal warm air advection to the east away from heating perturbation. Figure 12a shows the difference in horizontal temperature advection between the warm eastern North Atlantic SSTA case. A negative perturbation forms west of the heating at 40°N and a positive perturbation to the east. Figure 12b shows the adiabatic cooling for the same case. Perturbations near 40°N are smaller than the perturbations in Fig. 12a, indicating the importance of horizontal temperature advection at midlatitudes in balancing the low-level heating. This is in contrast to the Gulf of Guinea SSTA case, in which perturbation vertical velocities (a weakening of the subsidence) balance the low-level heating. Figure 12c shows the difference in horizontal temperature advection between the warm Gulf of Guinea SSTA case and the control. Figure 12d shows the difference in adiabatic cooling for the warm Gulf of

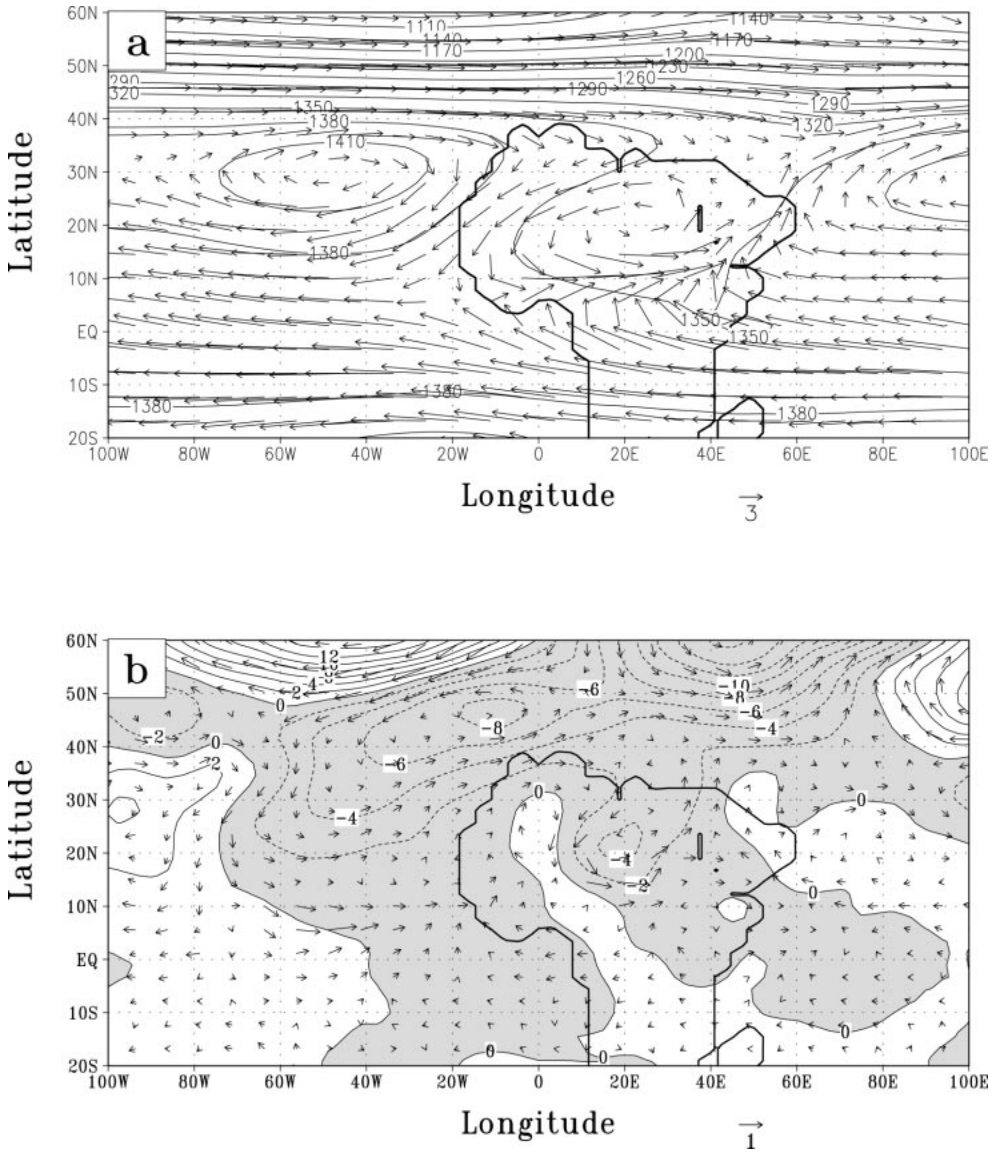

FIG. 11. (a) The 866-mb eddy geopotential and eddy winds for the GCM control integration. (b) Warm eastern North Atlantic SSTA simulation minus the control for 866-mb eddy geopotential and eddy wind differences. Contour units are gpm, and the vector scale is m s^{-1}. Negative perturbations of eddy geopotential are shaded.

Guinea case. Perturbation values are centered over the heating region and are roughly three times larger than the horizontal perturbation values.

Farther south adiabatic cooling becomes a more important mechanism for balancing the low-level heating. Subsidence over the heating weakens, and low-level heights fall over the SSTA and along 10°N, while over the western North Atlantic between 70° and 100°W heights rise.

The mixing ratio over the warm SSTAs increases, and much of the moisture is transported into middle latitudes by the basic-state westerly flow. The rest of the moisture from SSTAs is advected equatorward in the anticyclonic circulation. Some of the added moisture penetrates onto West Africa between the Greenwich meridian and the west coast, but most is advected westward into the ITCZ. Rainfall is enhanced along 10°N, from the Greenwich meridian to about 60°W, due to the higher mixing ratios and stronger upward vertical motions.

Figure 13 shows the difference in eddy geopotential heights and winds at 866 mb between the cold eastern North Atlantic SSTA case and the control. The North Atlantic anticyclone strengthens over the cold eastern Atlantic SSTAs, expanding over northwest Africa. Low-level heights increase over the eastern North Atlantic, extending eastward over northwest Africa.

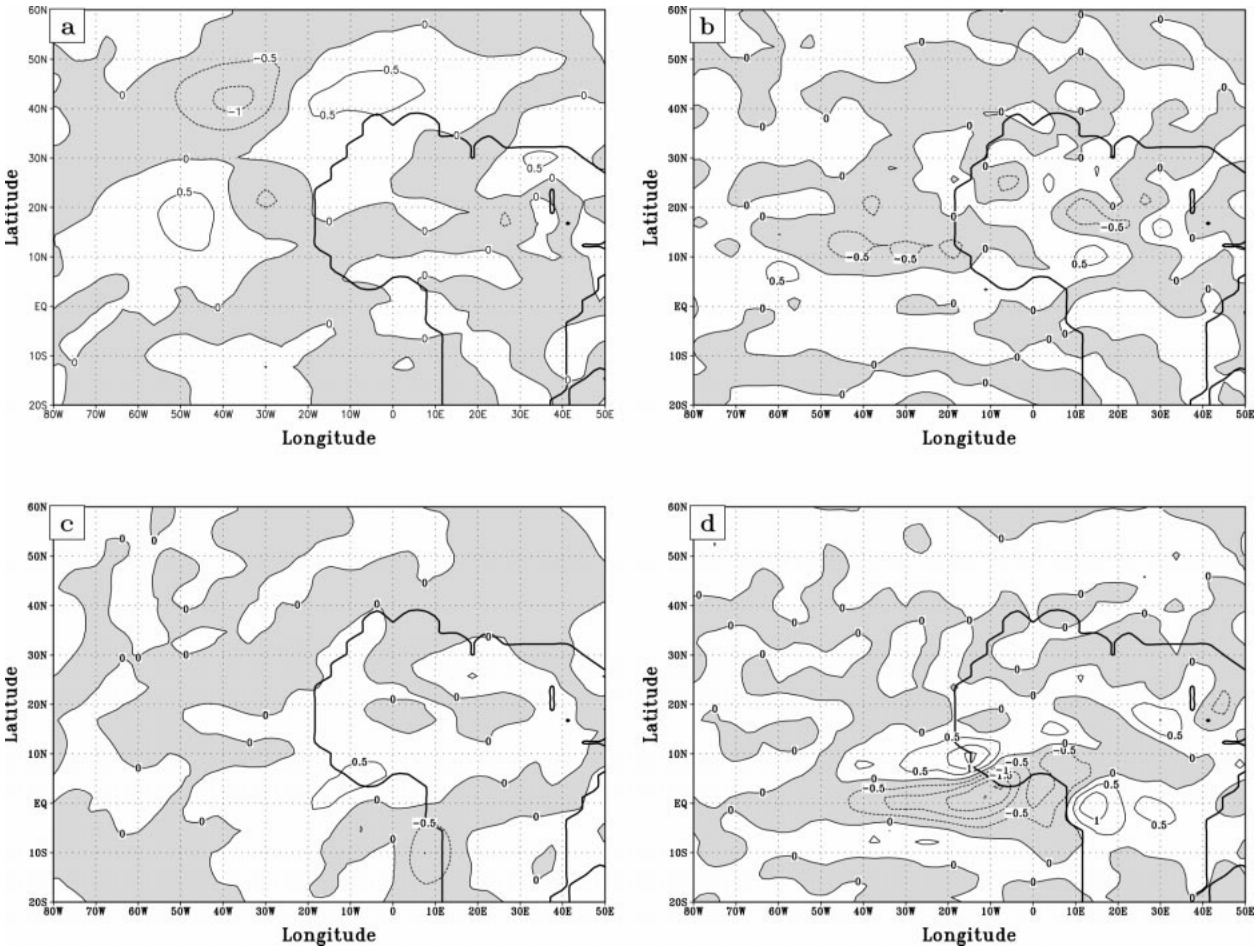

FIG. 12. The 935-mb warm eastern North Atlantic SSTA simulation minus the control (a) horizontal temperature advection and (b) adiabatic cooling differences. The 935-mb warm Gulf of Guinea SSTA simulation minus the control (c) horizontal temperature advection and (d) adiabatic cooling differences. Contour intervals are every 0.5 K day^{-1} with negative perturbations shaded.

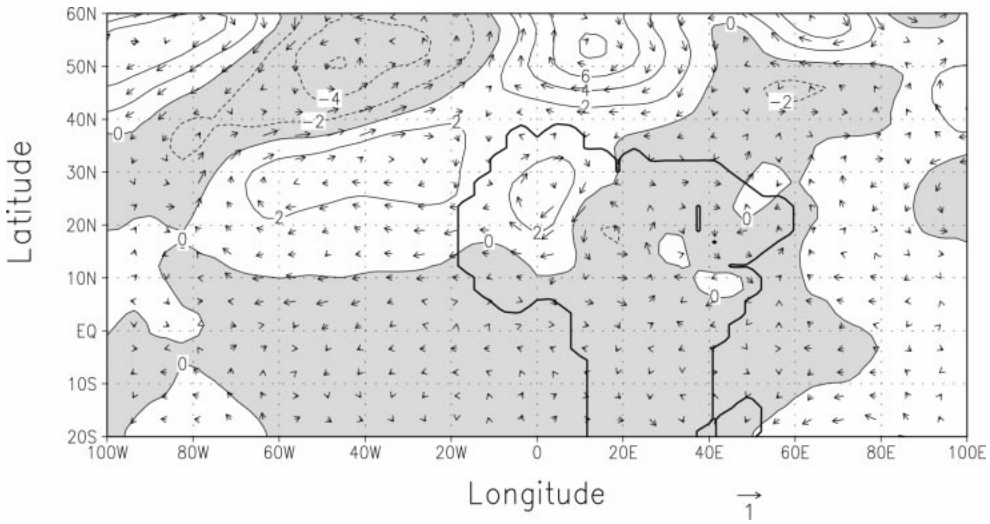

FIG. 13. Cold eastern North Atlantic SSTA simulation 866-mb eddy geopotential and eddy wind anomalies. Units are gpm for eddy geopotential, m s^{-1} for the eddy wind. Negative eddy geopotential perturbations are shaded.

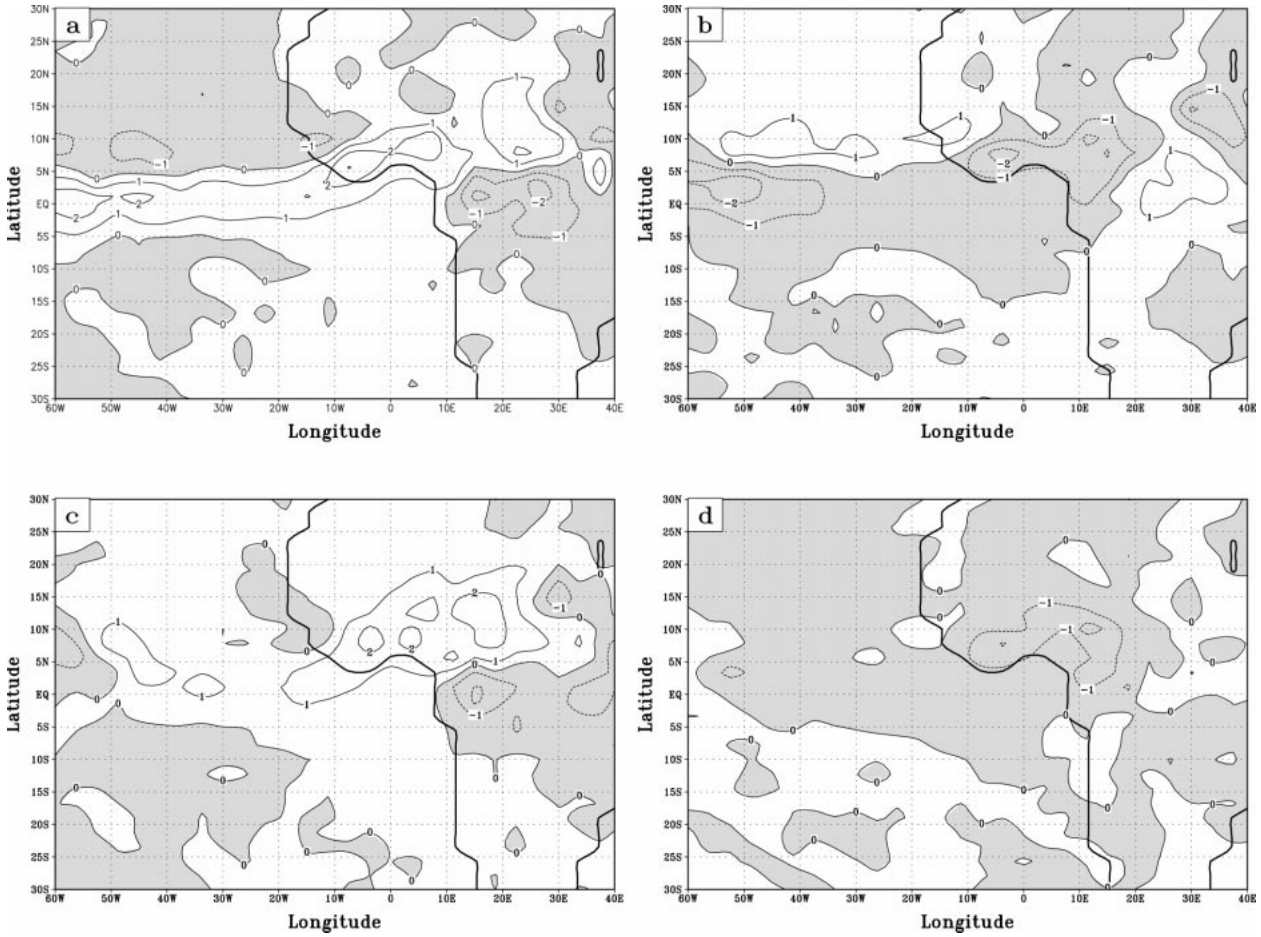

FIG. 14. Differences from the GCM control precipitation for (a) the warm Gulf of Guinea–cold Eastern North Atlantic SSTAs case, (b) the cold Gulf of Guinea–warm Eastern North Atlantic SSTAs case, (c) the warm Gulf of Guinea–warm eastern North Atlantic SSTAs case, and (d) the cold Gulf of Guinea–cold eastern North Atlantic SSTAs case. Units are mm day^{-1} and shading denotes negative perturbations.

An examination of the thermodynamic budget shows that the atmosphere responds to anomalous cooling over the eastern North Atlantic near 40°N and 30°W by increasing the advection of warm air from the west and southwest and by increasing the advection of cooler air eastward away from the region. Between 10° and 20°N adiabatic warming is more important. Anomalous subsidence weakens the upward vertical motions over the eastern North Atlantic along 10°N, while farther south, over the equatorial Atlantic subsidence is reduced.

The mixing ratio over the cold SSTAs decreases as evaporation over the SSTAs is reduced. Relatively drier air is advected equatorward in the anticyclonic circulation. Rainfall is reduced along 10°N over the Atlantic due to the reduced moisture content of the atmosphere and the weaker upward vertical motions.

7. Response to combined SSTA cases

In general, the stronger response to Gulf of Guinea SSTAs dominates in the combined SSTA cases. Figures 14a–d show the anomalous rainfall for the warm Gulf of Guinea–cold eastern North Atlantic, the cold Gulf of Guinea–warm eastern North Atlantic, the warm Gulf–warm eastern North Atlantic, and the cold Gulf–cold eastern North Atlantic SSTA cases, respectively. The differences from the Gulf of Guinea only SSTA precipitation perturbations (Figs. 6a and 6b) are relatively minor. Notable differences are discussed below.

The combination of cold eastern North Atlantic and warm Gulf of Guinea SSTAs results in a modification of the magnitudes of the rainfall anomalies associated with the warm Gulf of Guinea SSTAs alone. Figure 14a shows the difference between the precipitation field with these two SSTAs and the control. Negative rainfall perturbations along 10°N over the eastern North Atlantic and positive rainfall perturbations along the equator over the Atlantic are larger in magnitude than the corresponding precipitation anomalies from the warm Gulf of Guinea SSTA only case. In the thermodynamic budget (not shown), negative perturbation vertical velocities (a weakening of upward vertical motions) balance the low-level cooling over the eastern North Atlantic, north of the ITCZ. Mixing ratios north of the ITCZ over the

Atlantic are also lower than the warm Gulf of Guinea SSTA alone simulation's mixing ratios. Compared to the warm Gulf of Guinea SSTA only case rainfall is reduced more along 10°N from the Greenwich meridian to 70°W due to the lower mixing ratios and weaker upward vertical motions.

Figure 14b shows the rainfall difference between the cold gulf–warm eastern North Atlantic SSTA case and the control (Table 1). Magnitudes of the rainfall perturbations between 10°N and the equator over the Atlantic Ocean are larger than the warm Gulf of Guinea SSTA alone simulation (Fig. 6b). Positive perturbation vertical motions near 10°N balance the low-level heating, while mixing ratios are larger than in the cold Gulf of Guinea SSTA alone case over the North Atlantic, leading to a bigger positive rainfall perturbation along 10°N. Over the equatorial Atlantic, negative rainfall perturbations are about 25% larger than the cold Gulf of Guinea SSTA case.

Figure 14c shows the precipitation difference between the warm gulf–warm eastern North Atlantic SSTA case and the control. Positive rainfall perturbations over the western Sahel are larger than in the warm Gulf of Guinea SSTA case. The Gill-like atmospheric response described in section 5 is about twice as strong as the response to the warm Gulf of Guinea SSTA alone case. Compared to the control simulation, heights are lower over eastern North Atlantic and the thermal gradient is reduced between West Africa and the eastern North Atlantic. Subsidence is weaker than in the control over both the Gulf of Guinea and the eastern North Atlantic, while moisture content of the atmosphere over the western Sahel is about three to five times larger than the warm Gulf of Guinea SSTA case.

Over the eastern North Atlantic north of 10°N, positive precipitation perturbations replace the negative perturbations found in the cold Gulf of Guinea SSTA only case. Anomalous adiabatic cooling balances the low-level heating over the eastern North Atlantic, weakening the subsidence over the eastern North Atlantic, while strengthening the upward vertical motions in the ITCZ.

Figure 14d shows the precipitation difference between the cold gulf–cold eastern North Atlantic SSTA case and the control simulation (Table 1). Negative precipitation perturbations along the Guinean coast are smaller than in the cold Gulf of Guinea SSTA alone case. The addition of the cold eastern North Atlantic SSTAs strengthens the atmospheric response obtained from the cold Gulf of Guinea SSTA case described in section 5. Compared to the cold Gulf of Guinea alone SSTA case, the anticyclonic perturbation over West Africa is about 25% stronger. Heights are higher over the eastern North Atlantic as the North Atlantic high intensifies. Compared to the control simulation the land–sea thermal gradient between Africa and the North Atlantic and subsidence over the eastern North Atlantic and Gulf of Guinea are stronger. The moisture content of the atmosphere over the North and South Atlantic is lower than in the control due to the reduced evaporation over the SSTAs.

In general, the superposition of the perturbations from the Gulf of Guinea and eastern North Atlantic SSTA simulations are not equivalent to anomalies from the combined Gulf of Guinea–eastern North Atlantic SSTA cases (Table 1). For example, Fig. 15 shows the superposition of the rainfall differences between the warm Gulf of Guinea SSTA case and the control and the warm eastern North Atlantic SSTA case and the control. Rainfall perturbations in the superposition case have larger magnitudes than the perturbations for the combined SSTA case. Unlike the combined SSTA case, negative perturbations are present over the Sahel between the Greenwich meridian and 20°E and over the eastern North Atlantic along 10°N.

The differences in the precipitation perturbations between the superposition of the isolated cases and the combined SSTA simulation arise because of nonlinearities in the low-level flow field, which are introduced when SSTAs are simultaneously present in the Gulf of Guinea and the eastern North Atlantic.

Figure 16a shows the superposition of the differences of the wind field at 866 mb between the warm Gulf of Guinea SSTA case and the control, and between the warm eastern North Atlantic SSTA simulation and the control. As in the warm Gulf of Guinea SSTA case (Fig. 9a), anomalous low-level flow is directed toward the warm Gulf of Guinea SSTAs along the equator, and northward into West Africa. Two distinct cyclonic perturbations are present over northern Africa, one over West Africa associated with the Rossby wave response to warm Gulf of Guinea SSTAs (Fig. 9a), and the other over central Sahara associated with the response to the warm eastern North Atlantic SSTAs (Fig. 11b).

Figure 16b shows the wind differences between the warm gulf–warm eastern North Atlantic SSTA case and the control (Table 1). Unlike the superposition case, the two cyclonic perturbations blend into a single large cyclonic perturbation over West Africa. Anomalous southerlies converge with anomalous northerlies over Niger in the superposition case (Fig. 16a). In the warm gulf–warm eastern North Atlantic SSTA case, interactions between these flow anomalies result in an anomalous low-level flow that is more westerly over the Guinean coast and Sahel. This has an impact on the latent heating field over West Africa, since the southerly flow from the Gulf of Guinea is important in supplying moisture to West Africa. Mixing ratio contours from the control simulation are also shown in Fig. 16b. The structure of this field is predominantly zonal, with the largest mixing ratios found in the vicinity of the ITCZ along 12°N. Unlike the superposition case, more moisture is transported eastward into the central Sahel in the warm gulf–warm eastern North Atlantic SSTA simulation, ultimately leading to larger latent heating rates over this region.

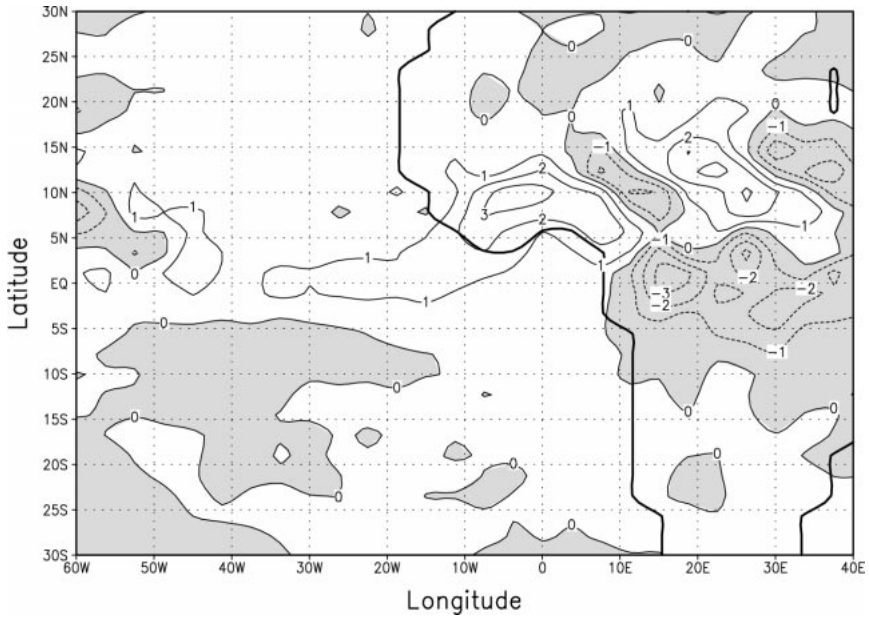

FIG. 15. Superposition of the precipitation anomalies from the warm Gulf of Guinea SSTA case and the warm eastern North Atlantic SSTA case. Units are mm day^{-1} and shading denotes negative perturbations.

The dipole precipitation perturbation structure over the Sahel and the Guinean coast is identified in observational studies (e.g., Janicot 1992; Fontaine and Bigot 1993; Rowell et al. 1995) when either a cold Gulf of Guinea–warm eastern North Atlantic or a warm Gulf of Guinea–cold eastern North Atlantic SSTA pattern occurs in the GCM simulations. The rainfall dipole response is present in the isolated Gulf of Guinea SSTA cases, but is stronger in the warm gulf–cold eastern North Atlantic and the cold gulf–warm eastern North Atlantic SSTA cases, where eastern North Atlantic SSTAs reinforce the dynamical response associated with the Gulf SSTAs.

The dynamics leading to the dipole response in these cases (cold–warm and warm–cold) is similar to that for the warm and cold gulf cases of section 5. For example,

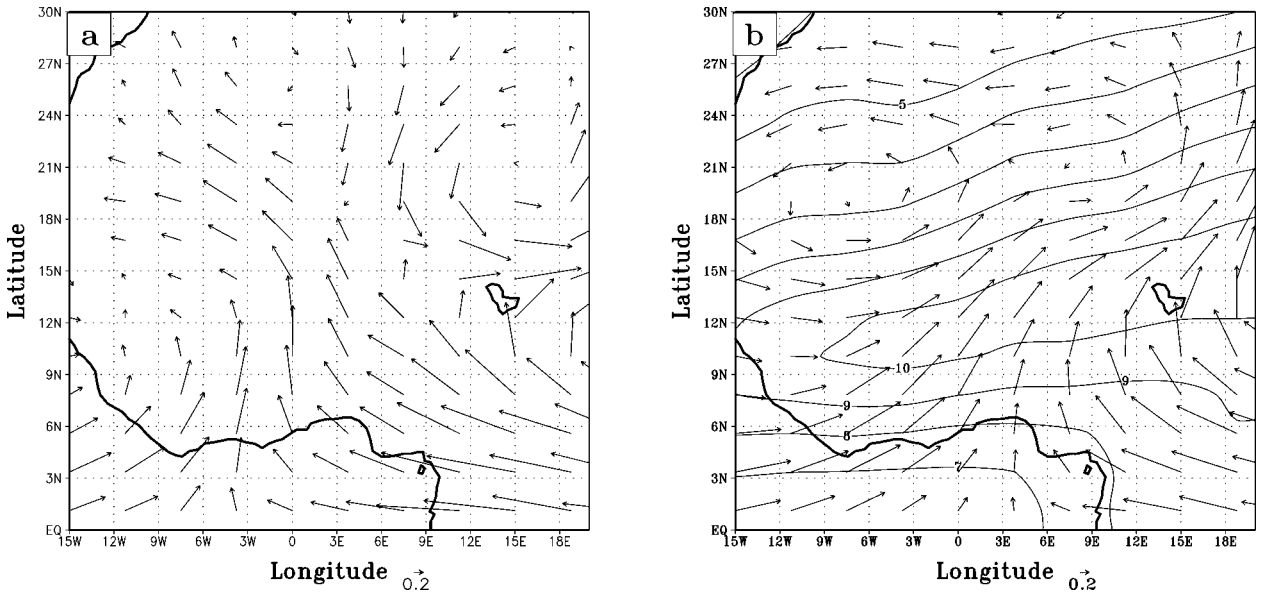

FIG. 16. (a) Superposition of the 866-mb wind anomalies from the warm Gulf of Guinea SSTA and the warm eastern North Atlantic SSTA cases. (b) The 866-mb mixing ratio from the control simulation and wind anomalies from the warm Gulf of Guinea–warm eastern North Atlantic SSTA case. The contour units are g_{H2O} kg^{-1} and vector scale is m s^{-1}.

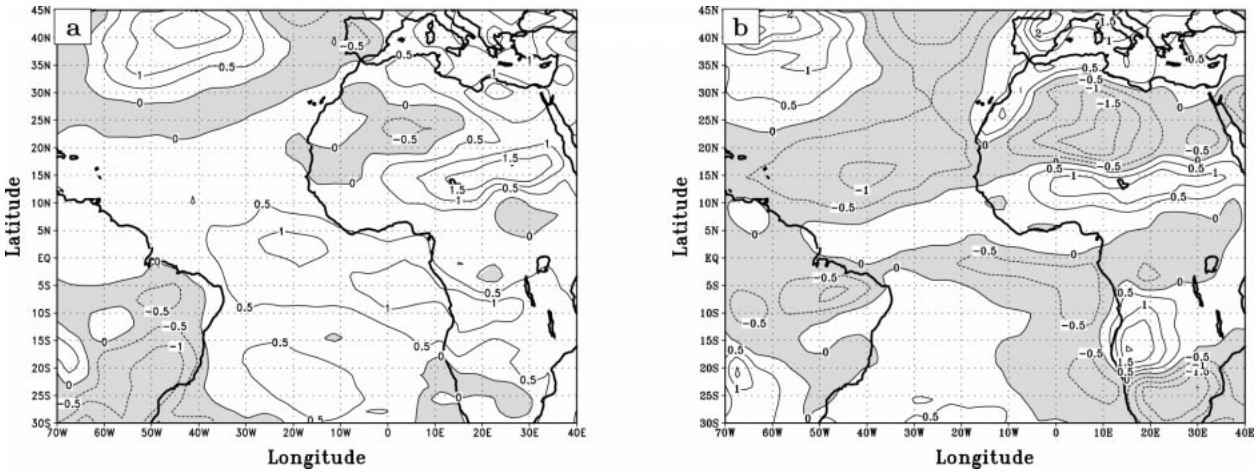

FIG. 17. Summer (JJA) surface temperature differences between the 1949 and 1998 NCEP average and the summer of (a) 1988 and (b) 1994. Units are K and negative values are shaded.

when warm SSTAs are present in the gulf, there is an increase (decrease) in advection of lower (higher) planetary vorticity air from the south (north) and the low-level wind convergence is stronger (weaker) over the Guinean coast (Sahel). This leads to more (less) rainfall over the Guinean coast (Sahel). Over the Guinean coast, this mechanism instigates a positive feedback to strengthen the monsoon flow from the Gulf of Guinea. Over the Sahel, it is unclear from these climatological simulations whether this mechanism instigates a positive or negative feedback.

8. Comparison with the summers of 1988 and 1994

It would be very difficult, and probably impossible, to conduct the above analysis on the observations. While excellent ground-based precipitation datasets are available for the last 100 yr or more (Nicholson 1980) these datasets do not cover the adjacent oceans. But one would also need information about atmospheric moisture, low-level winds, and evaporation rates for the land surface and nearby oceans to conduct the moisture budget analysis, and these are not available for the long timescales and resolution needed.

On the other hand, restricting our analysis to the GCM output is unsatisfying. Two summer seasons (1988 and 1994) are used to explore the degree to which we can attribute observed precipitation perturbations to observed SSTAs guided by the analysis from the idealized GCM. SSTAs from Reynolds and Smith (1994), as prescribed in the NCEP reanalysis and the satellite-gauge precipitation dataset, are used to determine which summer seasons to compare.

We choose the summers of 1988 and 1994 because of their contrasting SSTA and precipitation distributions. The summer of 1988 was wet over the Sahel and southern Sahara, and was one of only two years in the 1980s where the annual rainfall exceeded the mean rainfall (Nicholson 1993). During 1988, the ENSO cycle was in a cold phase. The summer of 1994 from June to early August was relatively dry over the western and southern Sahel and along the Guinean coast (Nicholson et al. 1996). Unusually heavy rains occurred over the Sahel late in the season, lasting into October, making the year of 1994 one of the wettest years over the Sahel in the past 30 yr. Note that our choice of definition for ''summer season'' excludes the months of September and October, therefore in the summer season of 1994 the western Sahel and Guinean coast are drier than normal. This definition of ''summer'' may be too rigid, missing the character of the late summer climate interactions.

Figure 17a shows the surface temperature differences between the summer of 1988 and the 1949–98 summer climatology. Warm SSTAs are present over the Gulf of Guinea and the eastern North Atlantic in 1988. This case is analogous to the warm gulf–warm eastern North Atlantic SSTA GCM simulation (Fig. 14c). Figure 17b shows the surface temperature differences between the summer of 1994 and the climatology. Cold SSTAs are present over both the Gulf of Guinea and eastern North Atlantic in 1994, analogous to the cold gulf–cold eastern North Atlantic SSTA case (Fig. 14d). Remember, however, that the magnitudes of the SSTAs are much larger in the model.

Figure 18a shows the precipitation difference between the summer of 1988 and the summer of 1994 from the satellite-gauge precipitation product. Rainfall is greater in the summer of 1988 over the Atlantic from 60°W to 10°E between the equator and 10°N. This includes the Guinean coast where precipitation rates are about 2 mm day^{-1} larger in 1988 than 1994. Rainfall is greater in the summer of 1994 over the northern Sahel.

Figure 18b shows the rainfall differences between the summer of 1988 and the summer of 1994 from the

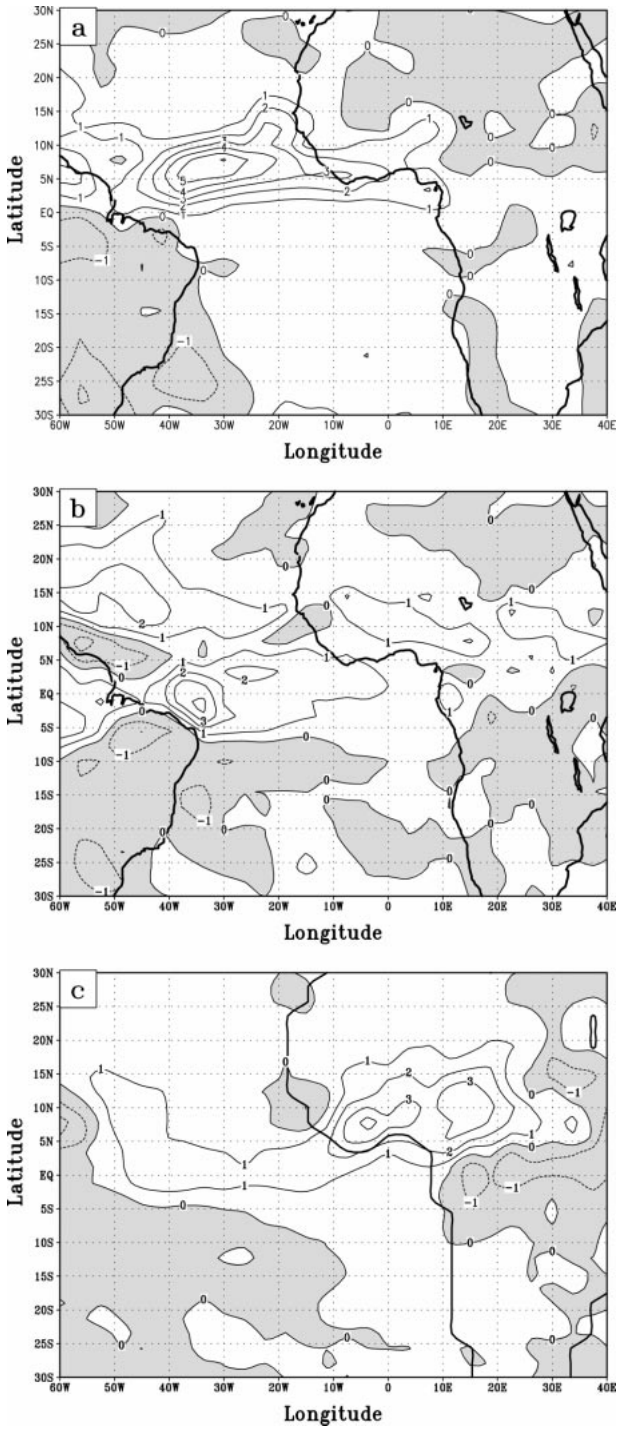

FIG. 18. Summer of 1988 precipitation minus summer of 1994 precipitation from the (a) satellite-gauge precipitation product from Huffman et al. (1995) and (b) NCEP reanalysis. (c) Model rainfall differences between the warm Gulf of Guinea–warm eastern North Atlantic SSTA and the cold Gulf of Guinea–cold eastern North Atlantic SSTA simulations. Contour interval is 1 mm day^{-1}. Shading denotes negative perturbations.

NCEP reanalysis. Rainfall is greater in the summer of 1988 than in 1994 over West Africa along 10°N, and over the equatorial Atlantic. Unlike the rainfall from the satellite-gauge product, precipitation rates in the reanalysis are greater over East Africa and northern Sahel in the summer of 1988. This discrepancy may be due to the wet bias of the NCEP reanalysis in the lower and middle troposphere discussed in section 4.

Figure 18c shows the GCM simulation precipitation difference between the warm Gulf of Guinea–warm eastern North Atlantic SSTAs case and the cold Gulf of Guinea–cold eastern North Atlantic SSTA case. The rainfall perturbations are similar to the anomalies generated in the warm Gulf of Guinea SSTA simulation discussed in section 5, but with magnitudes amplified. Over the Guinean coast region, the precipitation perturbations are approximately twice as large as in the observations (Fig. 18a) and the reanalysis (Fig. 18b). Positive precipitation anomalies over the Sahel are similar to the anomalies in the reanalysis, but magnitudes are larger in the model. The larger precipitation perturbations over the Guinean coast and West Africa in the model may be due to the larger SSTA magnitudes. Over the equatorial Atlantic, the positive anomalies in the model are similar to the large-scale anomalies in the observations, but with smaller perturbation magnitudes. Unlike the satellite-gauge rainfall observations (Fig. 18a) and reanalysis (Fig. 18b), precipitation was greater in the summer of 1988 over the Sahara in the model. This difference is most likely due to the absence of Europe in the model. The ''far-field'' response, between 10° and 40°E, does not occur in the satellite-gauge rainfall observations, and neither does the decrease over East Africa. The former discrepancy may be due to the absence of South America, and the latter to the lack of East African topography in the model. The enhancement of rainfall along 10°N over the North Atlantic in the observations is hinted at in the GCM, but again the magnitudes are subdued in the GCM despite the larger SSTA magnitudes.

The moisture budget analyses for the NCEP reanalysis and the GCM are shown in Fig. 19. The moisture convergence term differences for the reanalysis and the GCM are shown in Figs. 19a and 19b, respectively. The presence of more small-scale structure in the reanalysis is expected, but there are features common with the GCM. Positive anomalous moisture convergence occurs over the Guinean coast and along the equator between the Greenwich meridian and 40°W in both the reanalysis and the GCM, with larger anomaly magnitudes found in the model. Negative anomalous moisture convergence also occurs in both the reanalysis and the GCM over the Congo basin. Negative anomalous moisture convergence located over the west coast of Africa along 10°N in the GCM is weak in the reanalysis, and positioned farther to the west. As in the model, the moisture convergence term is responsible for most of the structure of the precipitation perturbation in the NCEP reanalysis.

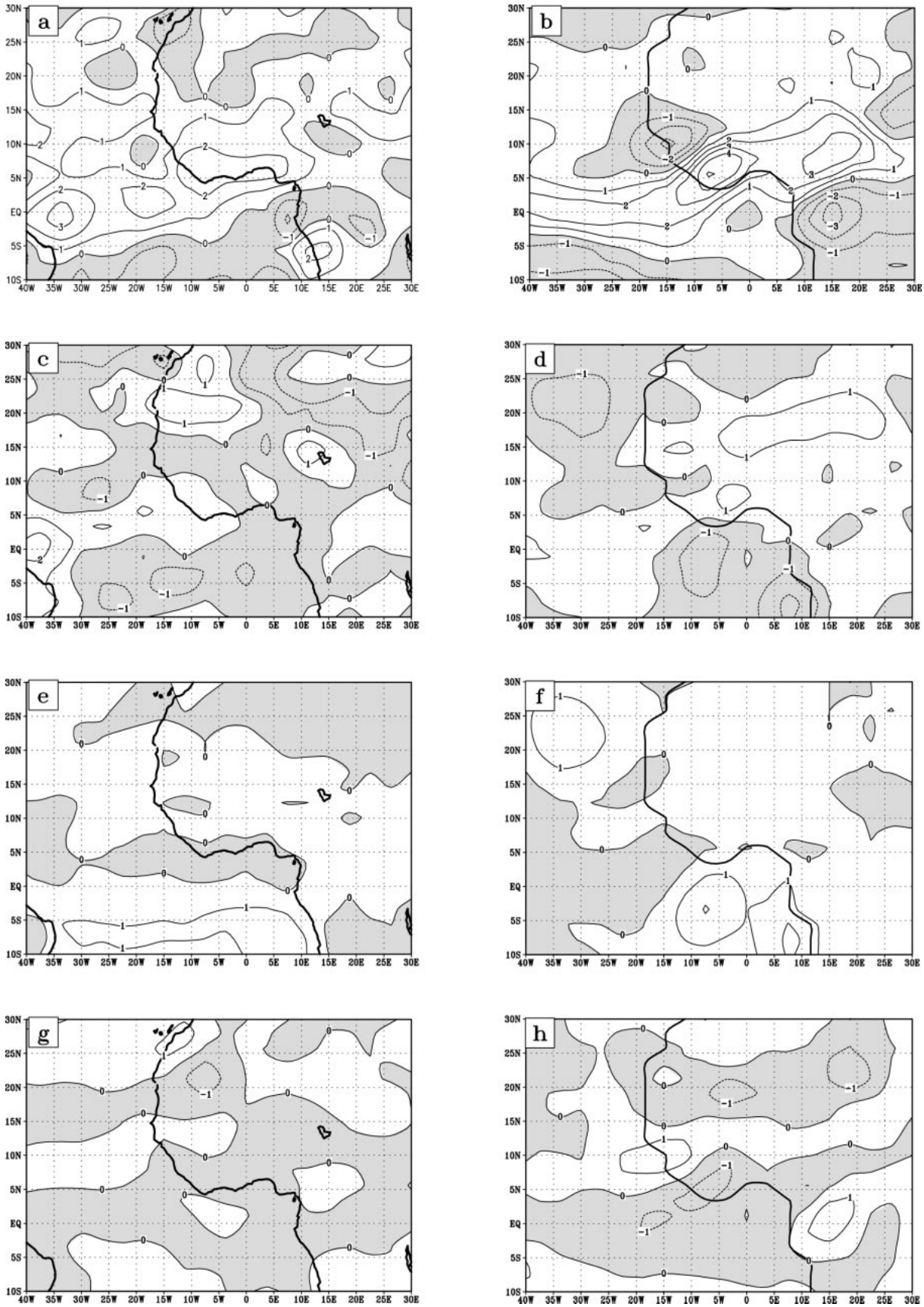
a
b
c
d
e
f
g
h
30N
25N
20N
15N
10N
5N
EQ
5S
10S
40W 35W 30W 25W 20W 15W 10W 5W 0 5E 10E 15E 20E 25E 30E

The moisture advection term differences in the reanalysis (Fig. 19c) also have features in common with the GCM model differences (Fig. 19d). Both the reanalysis and the model produce negative perturbations over the Gulf of Guinea and the eastern North Atlantic, and positive perturbations over the western Sahel (west of Greenwich). Magnitudes of the perturbations in the reanalysis are comparable to the modeled magnitudes. Discrepancies in the moisture advection term occur over the rest of northern Africa due to differences in the perturbational flow. Unlike the model, the anomalous southerly flow from the Gulf of Guinea does not extend over the Sahel and central Africa. Note, interpretations drawn from the moisture budget terms dependent on mixing ratio over the Sahel and Sahara are inconclusive due to the wet bias of the reanalysis over these regions. This bias was discussed in section 4.

Evaporation differences in the reanalysis (Fig. 19e) generally agree with the differences obtained from the model results (Fig. 19f). Positive evaporation perturbations occur over the eastern North Atlantic and Gulf of Guinea SSTA regions. Magnitudes are larger in the model, reflecting the larger SSTA magnitudes chosen for these GCM simulations.

As in the isolated Gulf of Guinea (Fig. 7) and eastern North Atlantic SSTA cases, the largest perturbations in the moisture advection term and evaporation occur over the SSTAs and downwind of the eastern North Atlantic SSTAs over the central North Atlantic Ocean. Their perturbation fields do not resemble the structure of the precipitation perturbation, but both terms are important factors in determining the anomalous rainfall over the Atlantic Ocean.

Figures 19g and 19h show the moisture transient term differences in the reanalysis and the model, respectively. Similar to the model differences, positive perturbations are found along 10°N, west of 10°W, and negative perturbations are located over the Guinean coast and northwestern Sahel in the reanalysis. The positive perturbation over the Congo in the model is weaker in magnitude and about 5° farther north in the reanalysis. In general, the magnitudes of the perturbations in the reanalysis are smaller than the model anomalies.

The residual term differences between the summer of 1988 and 1994 for the reanalysis are shown in Fig. 20. The orographic term is included in the residual term because it is difficult to obtain an accurate estimate of this term from the reanalysis. Residual perturbations are located along the west coast of Africa and are associated with the Guinean and Cameroon coastal highlands, possibly suggesting the importance of the orographic term in determining the anomalous rainfall. Residual perturbations over the Atlantic Ocean in Fig. 20 suggest that maybe the convergence and/or advection term are in error. Computing the moisture budget on sigma surfaces, which are not available for the NCEP climatology, would improve the estimate of the moisture budget terms.

As in the GCM SSTA simulations in sections 5 and 6, differences in the column moisture budget are related to differences in the moisture content of the atmosphere as well as the dynamical response of the atmosphere. The water vapor content of the atmosphere is greater over the North Atlantic and West Africa in the summer of 1988. This includes the equatorial Atlantic and Guinean Coast, where mixing ratios are about 1 gm kg^{-1} greater in 1988 than 1994. Over the Congo basin and equatorial Africa the water vapor content of the atmosphere is smaller in 1988.

The Gill response identified in the warm Gulf of Guinea SSTA simulation (Fig. 9a) is not discernable in the reanalysis. Even so, perturbations over the Guinean Coast in the low-level flow field from the reanalysis resemble perturbations identified in the warm Gulf SSTA case. Figure 21 shows the geopotential and eddy wind differences of the reanalysis between the summer of 1988 and the summer of 1994 at 850 mb. As in the warm Gulf of Guinea SSTA case (Fig. 9a), the perturbation winds indicate that flow from the Gulf of Guinea onto the Guinean coast is stronger when warm SSTAs are located in the Gulf of Guinea. Unlike in the warm Gulf of Guinea SSTA simulation, the anomalous flow over the western Sahel is westerly in the reanalysis and is associated with a cyclonic perturbation over northwest Africa. The large magnitude of this perturbation suggests that it may be a response to an extratropical or midlatitude forcing, and possibly explains why the Rossby response to warm Gulf of Guinea SSTAs is not discernable over West Africa. Over the equatorial Atlantic Ocean anomalous flow is eastward, directed toward the warm Gulf of Guinea SSTAs, which agrees with results from section 5. To the east of the Gulf of Guinea SSTA region, no Kelvin wave response is noticeable.

The agreement between the precipitation perturbations may be spurious since only two summers were

←

FIG. 19. Anomalous moisture convergence term for (a) the NCEP reanalysis summer of 1988 minus the summer of 1994 and (b) the warm gulf–warm eastern North Atlantic SSTA minus the cold gulf–cold eastern North Atlantic SSTA simulations. Anomalous moisture advection term for (c) the NCEP reanalysis summer of 1988 minus the summer of 1994 and (d) the warm gulf–warm eastern North Atlantic SSTA minus the cold gulf–cold eastern North Atlantic SSTA simulations. Anomalous evaporation for (e) the NCEP reanalysis summer of 1988 minus the summer of 1994 and (f) the warm gulf–warm eastern North Atlantic SSTA minus the cold gulf–cold eastern North Atlantic SSTA simulations. Anomalous moisture transients for (g) the NCEP reanalysis summer of 1988 minus the summer of 1994 and (h) the warm gulf–warm eastern North Atlantic SSTA minus the cold gulf–cold eastern North Atlantic SSTA simulations. Contour interval is 0.5 mm day^{-1}, except for the moisture convergence term, where it is 1 mm day^{-1}. Shading denotes negative perturbations.

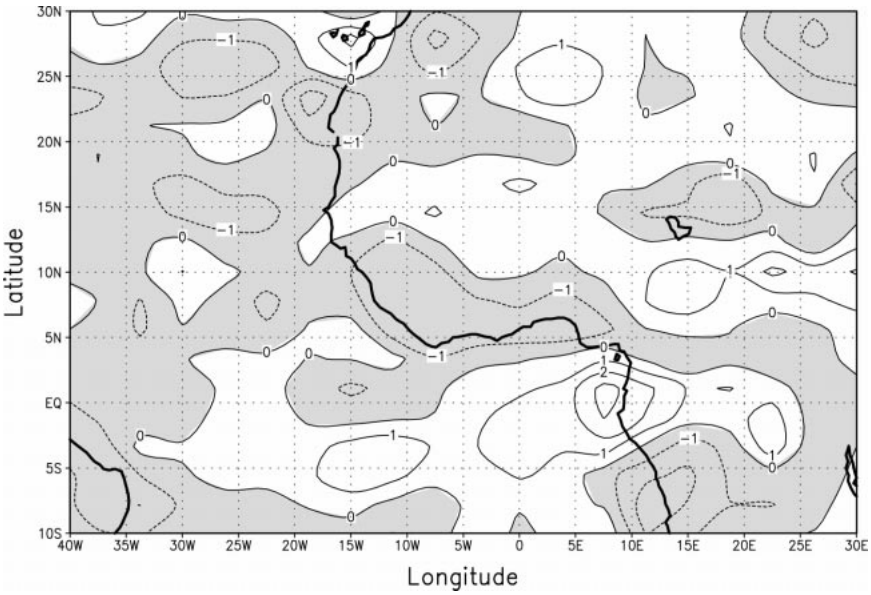

FIG. 20. NCEP reanalysis atmospheric water vapor budget residual–orographic term difference for the summer of 1988 minus the summer of 1994. Units are mm day^{-1} and negative values are shaded.

considered in the reanalysis, and the reanalysis contains many possible causes of precipitation anomalies (e.g., global SSTAs). Janicot et al. (1996) and Ward (1998) suggest that global SSTAs in the Tropics are associated with Sahelian rainfall via a global tropical circulation, especially during ENSO events. However, the focus on the ''near-field'' response to SSTAs makes the comparison stronger. Trzaska et al. (1996) concluded that Atlantic SST forcing combined with global SST forcing in their atmospheric GCM led to a significant modulation of the climate signal over northern tropical Africa by reducing the impact of ENSO forcing. In addition, a comparison of the vertically profiled GCM simulated and reanalyzed anomalous moisture convergence (not

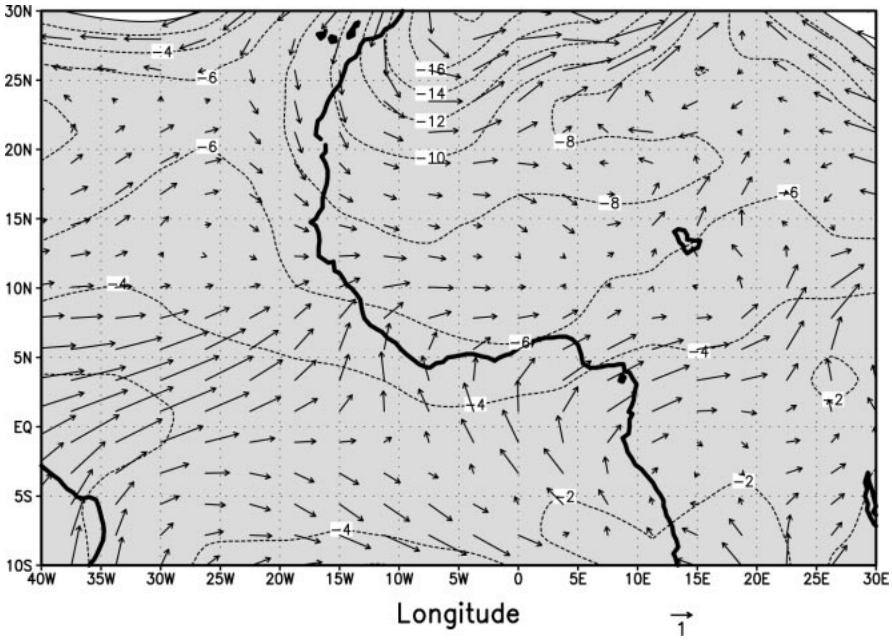

FIG. 21. NCEP reanalysis 850-mb geopotential and eddy wind differences between the summer of 1988 and the summer of 1994. Contour units are gpm and the vector scale is m s^{-1}. Negative values are shaded.

shown) suggests that the dynamical support for the precipitation anomalies is similar in the model and reanalysis. For example, both produce anomalous low-level moisture convergence over the Gulf of Guinea, extending over the Guinean coast and peaking at around 850 mb over the ITCZ axis. The low-level southerly onshore flow associated with the midtropospheric heating and vortex stretching aloft is stronger in the summer of 1988 than 1994, feeding moisture-laden air into the ITCZ from the south. The enhanced low-level flow of relatively ''wetter'' air is necessary to maintain the midtropospheric heating and the low-level flow, and results in the increase of moisture convergence along the Guinean coast.

9. Summary and conclusions

An atmospheric GCM with idealized prescribed boundary conditions is used to examine the sensitivity of West African rainfall to SSTAs in the Gulf of Guinea and the eastern North Atlantic Ocean during the boreal summer. A series of nine perpetual-July, 3600-day, R30 GCM simulations are analyzed to understand the response of the precipitation field and its relationship to the SSTAs through the large-scale circulation anomalies. We do not imply that Atlantic SSTAs solely explain anomalous rainfall over West Africa. Other factors, such as global SSTAs (Folland et al. 1986; Janicot et al. 1996; Ward 1998) and land surface conditions (Nicholson 1993; Cook 1997), have been associated with rainfall variability over West Africa. However, the response to regional SSTAs is known to be an important forcing of West African rainfall variability (e.g., Ward 1998), and we isolate the mechanisms of that variability in this paper. An overview of the results from the set of GCM simulations is summarized in three main conclusions.

a. The background circulation is an important determinant of the response to SSTAs over West Africa in summer

Rainfall increases along the Guinean coast and decreases over the Congo basin in response to warm Gulf of Guinea SSTAs because of the nature of the background circulation. These features in the precipitation perturbation can be largely understood in terms of the dynamical response to steady tropical forcing, namely, a Kelvin wave response along the equator and a Rossby wave response to the west of the SSTA. The Kelvin wave response is associated with a weakening of the equatorial Walker circulation, which has its up-branch over the Congo basin and its down-branch over the Gulf of Guinea. Anomalous low-level divergence occurs east of the SSTAs, which results in reduced precipitation rates over the Congo basin. The Rossby wave response is manifest as a strengthening of the West African monsoon and anomalous (upward) vertical velocities and increased rainfall over the Guinean coast region of West Africa.

The presence of the Walker circulation also has implications for the West African monsoon response. Subsidence over the Gulf of Guinea restricts deep vertical transport of water vapor over the warmed ocean surface and supports the poleward transport of moisture by the monsoon flow. This is one reason why the precipitation perturbations are not located over the SSTAs. However, it is possible that a large enough positive SSTA in the Gulf of Guinea could weaken the Walker circulation and subsidence enough so convection would break through directly over the SSTAs. If this occurred, the response to warm Gulf of Guinea SSTAs may include a precipitation reduction over West Africa instead of the precipitation increases simulated here.

Understanding the response to eastern North Atlantic SSTAs also requires a consideration of the ambient circulation. Rainfall over West Africa is generally insensitive to warm (cold) eastern North Atlantic SSTAs, except on the west coast where rainfall increases (decreases) within the ITCZ. Even with 3600-day averages, we did not capture a significant response in the precipitation field over land, although the precipitation response over the Atlantic was significant. There are two reasons for this reduced sensitivity over northern Africa. One is that horizontal advection is more effective in balancing anomalies at higher latitudes, and this type of dynamical response does not feed into the precipitation field as strongly as the more typical vertical (adiabatic) response in the Tropics. Also, the low-level flow between the North Atlantic and West Africa is northerly and northeasterly, which tends to isolate the continent from the eastern North Atlantic. Thus, the largest precipitation perturbations associated with anomalous heating over the eastern North Atlantic SSTAs occur within the ITCZ.

b. The precipitation response to warm SSTAs is not the negative of the precipitation response to cold SSTAs over northern Africa

The precipitation response to cold Gulf of Guinea SSTAs is opposite to the warm Gulf SSTA case, but with weaker perturbations. According to the Clausius–Clapeyron relation, the saturation vapor pressure and, therefore, evaporation rates are less sensitive to cold surface temperature anomalies than to warm temperature anomalies, and this may account for part ($\sim$20%) of the difference in perturbation magnitudes. In addition, anomalous column moisture convergence by transient eddies is more influential when cold SSTAs are present. Compared to the warm SSTA simulation, magnitudes of large-scale moisture convergence anomalies over West Africa are about 35% smaller for the cold SSTA case, while magnitudes of anomalous moisture convergence by transient eddies are only about 15% smaller.

c. *The response to eastern Atlantic and Gulf of Guinea SSTAs together does not equal the sum of the responses to the SSTAs individually*

Given the fact that the response to Gulf of Guinea SSTAs is much stronger than the response to eastern North Atlantic SSTAs over West Africa, one might conclude that a knowledge of Gulf of Guinea SSTAs alone would be sufficient to predict precipitation anomalies (assuming the absence of other forcing). An equivalent deduction is that a linear superposition of the anomalies associated with Gulf of Guinea SSTs and the anomalies associated with eastern North Atlantic SSTs would be similar to the anomalies that result when both Gulf of Guinea and eastern North Atlantic SSTAs are present. However, we find that a superposition of the anomalies differs from the anomalous response to combined SSTAs in important ways. Nonlinearities are introduced when the atmosphere responds to both SSTAs together, yielding a different perturbation flow field over Africa than would result from the superposition of the corresponding isolated SSTAs. For example, with warm SSTAs in both the Gulf of Guinea and eastern North Atlantic, the two cyclonic perturbations that form over West Africa in the superposition case blend into a single, larger cyclone in the combined SSTA simulation. The resulting perturbation low-level flow is more westerly over the Guinean coast and Sahel in the combined SSTA case. This has a large impact on the precipitation over West Africa, since the southerly flow from the Gulf of Guinea is important in supplying moisture to West Africa.

Acknowledgments. The authors would like to thank the National Center for Atmospheric Research, which is sponsored by the NSF, for computing time and observational data presented in this study. Thanks to the National Centers for Environmental Prediction for supplying the reanalysis output presented in this study. Special thanks to the two anonymous reviewers for their comments. This research was supported by Grant ATM-9815419 from the NSF and represents a portion of EKV's M.S. thesis at Cornell University.

REFERENCES

Bah, A., 1987: Towards the prediction of Sahelian rainfall from sea surface temperatures in the Gulf of Guinea. *Tellus,* **39A,** 39–48.

Cadet, D., and N. Nnoli, 1987: Water vapour transport over Africa and the Atlantic during the summer 1979. *Quart. J. Roy. Meteor. Soc.,* **113,** 581–602.

Cook, K. H., 1994a: Mechanisms by which surface drying perturbs tropical precipitation fields. *J. Climate,* **7,** 400–413.

——, 1994b: Understanding perturbations of the intertropical convergence zone over tropical continents. *Global Precipitation and Climate Change,* M. Desbois and F. Desalmand, Eds., NATO ASI Series I, Vol. 26, North Atlantic Treaty Organization, 349–360.

——, 1997: Large-scale atmospheric dynamics and Sahelian precipitation. *J. Climate,* **10,** 1137–1152.

Druyan, L. M., 1991: The sensitivity of sub-Saharan precipitation to Atlantic SST. *Climatic Change,* **18,** 17–36.

——, and R. D. Koster, 1989: Sources of Sahel precipitation for simulated drought and rainy seasons. *J. Climate,* **2,** 1438–1446.

——, and S. Hastenrath, 1991: Modeling the differential impact of 1984 and 1950 sea surface temperatures on Sahel rainfall. *Int. J. Climatol.,* **11,** 367–380.

——, and ——, 1992: GCM simulation of the Sahel 1984 drought with alternative specifications of observed SST. *Int. J. Climatol.,* **12,** 521–526.

Folland, C. K., T. N. Palmer, and D. E. Parker, 1986: Sahel rainfall and worldwide sea temperatures. *Nature,* **320,** 602–607.

——, J. A. Owen, M. N. Ward, and A. W. Coleman, 1991: Prediction of seasonal rainfall in the Sahel region of Africa using empirical and dynamical methods. *J. Forecasting,* **10,** 21–56.

Fontaine, B., and S. Janicot, 1992: Wind field coherence and its variations over West Africa. *J. Climate,* **5,** 512–524.

——, and S. Bigot, 1993: West African rainfall deficits and sea surface temperatures. *Int. J. Climatol.,* **13,** 271–285.

——, and S. Janicot, 1996: Sea surface temperature fields associated with West African rainfall anomaly types. *J. Climate,* **9,** 2935–2940.

Gill, A. E., 1982: *Atmosphere–Ocean Dynamics.* Academic Press, 662 pp.

Hoskins, B. J., and D. J. Karoly, 1981: The steady linear response of a spherical atmosphere to thermal and orographic forcing. *J. Atmos. Sci.,* **38,** 1179–1196.

Huffman, G. J., R. F. Alder, B. Rudolf, U. Schneider, and P. R. Keehn, 1995: Global precipitation estimates based on a technique for combining satellite-based estimates, rain gauge analysis, and NWP model precipitation information. *J. Climate,* **8,** 1284–1295.

Janicot, S., 1992: Spatiotemporal variability of West African rainfall. Part II: Associated surface and airmass characteristics. *J. Climate,* **5,** 499–511.

——, V. Moron, and B. Fontaine, 1996: Sahel drought and ENSO dynamics. *Geophys. Res. Lett.,* **23,** 515–518.

Janowiak, J. E., 1988: An investigation of interannual rainfall variability in Africa. *J. Climate,* **1,** 240–255.

Kalnay, E., and Coauthors, 1996: The NCEP/NCAR 40-Year Reanalysis Project. *Bull. Amer. Meteor. Soc.,* **77,** 437–471.

Lamb, P. J., 1978: Case studies of tropical Atlantic surface circulation patterns during recent sub-Saharan weather anomalies: 1967 and 1968. *Mon. Wea. Rev.,* **106,** 482–491.

——, and R. A. Peppler, 1990: West Africa. *Teleconnections: Linkages between ENSO, Worldwide Climate Anomalies, and Societal Impacts,* M. H. Glantz, R. W. Katz, and N. Nicholls, Eds., Cambridge University Press, 121–189.

——, and ——, 1992: Further case studies of tropical Atlantic surface atmospheric and oceanic patterns associated with sub-Saharan drought. *J. Climate,* **5,** 476–488.

Lenters, J. D., and K. H. Cook, 1995: Simulation and diagnosis of the regional South American precipitation climatology. *J. Climate,* **8,** 2988–3005.

Mintz, Y., and G. K. Walker, 1993: Global fields of soil moisture and land surface evapotranspiration derived from observed precipitation and surface air temperature. *J. Appl. Meteor.,* **32,** 1305–1334.

Newell, R. E., and I. W. Kidson, 1984: African mean wind changes between Sahelian wet and dry periods. *Int. J. Climatol.,* **4,** 27–33.

Nicholson, S. E., 1980: The nature of rainfall fluctuations in subtropical West Africa. *Mon. Wea. Rev.,* **108,** 473–487.

——, 1989: African drought: Characteristics, casual theories and global connections. *Understanding Climate Change, Geophys. Monogr.,* No. 52, IUGG, 79–100.

——, 1993: An overview of African rainfall fluctuations of the last decade. *J. Climate,* **6,** 1463–1466.

——, M. B. Ba, and J. Y. Kim, 1996: Rainfall in the Sahel during 1994. *J. Climate,* **9,** 1673–1676.

Palmer, T. N., C. Brankovic, P. Viterbo, and M. J. Miller, 1992: Mod-

eling interannual variations of summer monsoons. *J. Climate,* **5,** 399–417.

Reynolds, R. W., and T. M. Smith, 1994: Improved global sea surface temperature analysis using optimum interpolation. *J. Climate,* **7,** 929–948.

Rowell, D. P., C. K. Folland, K. Maskell, J. A. Owen, and M. N. Ward, 1992: Modeling the influence of global sea surface temperatures on the variability and predictability of seasonal Sahel rainfall. *Geophys. Res. Lett.,* **19,** 905–908.

——, ——, ——, and M. N. Ward, 1995: Variability of summer rainfall over tropical North Africa (1906–92): Observations and modelling. *Quart. J. Roy. Meteor. Soc.,* **121,** 669–704.

Semazzi, F. H. M., N. H. Lin, Y. L. Lin, and F. Giorgi, 1993: A nested model study of the Sahelian climate response to sea surface temperature anomalies. *Geophys. Res. Lett.,* **20,** 2897–2900.

Shea, D. J., K. E. Trenberth, and R. W. Reynolds, 1990: A global monthly sea surface temperature climatology. NCAR Tech. Note NCAR/TN-345 + STR, 167 pp. [Available from National Center for Atmospheric Research, P.O. Box 3000, Boulder, CO 80307-3000.]

Shinoda, M., 1990a: Long-term variability of the tropical African rainbelt and its relation to rainfall in the Sahel and northern Kalahari. *J. Meteor. Soc. Japan,* **68,** 19–35.

——, 1990b: Long term Sahelian drought from the late 1960's to the mid 1980's and its relation to the atmospheric circulation. *J. Meteor. Soc. Japan,* **68,** 613–624.

——, and R. Kawamura, 1994: Tropical rainbelt, circulation, and sea surface temperatures associated with Sahelian rainfall trend. *J. Meteor. Soc. Japan,* **72,** 341–357.

Trzaska, S., V. Moron, and B. Fontaine, 1996: Global atmospheric response to specific linear combinations of the main SST modes. Part I: Numerical experiments and preliminary results. *Ann. Geophys.,* **14,** 1066–1077.

Wagner, R. G., and A. M. Da Silva, 1994: Surface conditions associated with anomalous rainfall in the Guinea coastal region. *Int. J. Climatol.,* **14,** 179–199.

Ward, M. N., 1998: Diagnosis and short-lead time prediction of summer rainfall in tropical North Africa at interannual and multidecadal timescales. *J. Climate,* **11,** 3167–3191.